

~~30  
1-19-87~~

5/2 11 340

CONF-8307107-4

SLAC-PUB-3262

November 1983

(T/E)

## MARK III RESULTS FROM SPEAR

Walter Toki  
Stanford Linear Accelerator Center  
Stanford University, Stanford, California 94305

Talk presented for the MARK III Collaboration<sup>†</sup>

### ABSTRACT

First results from the MARK III detector at SPEAR are presented based on 2.7 million  $J/\psi$  decays. The  $\eta_c$  is observed in three modes,  $J/\psi \rightarrow \gamma\eta_c$ ,  $(\eta_c \rightarrow p\bar{p}, \eta\pi^+\pi^-)$ , and  $\phi\phi$ . Using the  $\phi\phi$  mode, the  $\eta_c$  spin-parity is determined to be  $0^-$ . The known radiative  $J/\psi$  decays  $J/\psi \rightarrow \gamma f(f \rightarrow \pi^+\pi^-)$ ,  $\gamma\eta'(f' \rightarrow \gamma\rho^0, \eta\pi^+\pi^-)$ ,  $\gamma f'(f' \rightarrow K^+K^-)$ ,  $\gamma\theta(\theta \rightarrow K\bar{K})$ , and  $\gamma(\iota \rightarrow \pi K\bar{K})$  are observed and their branching ratios found to be in agreement with previous measurements. In the  $J/\psi \rightarrow \gamma K^+K^-$  mode a new state is observed at 2.22 GeV and in the  $J/\psi \rightarrow \gamma\gamma\rho^0$  and  $\gamma\eta\pi^+\pi^-$  modes evidence for new structures near 1.4 GeV is presented.

\* Work supported in part by the Department of Energy, contracts DE-AC03-76ER01195, DE-AM03-76SF00034 and DE-AC03-81ER40050.

<sup>†</sup> members of the MARK III Collaboration are R. M. Baltrusaitis, D. Coffman, J. Hauser, D. G. Hitlin, J. D. Richman, J. J. Russell, and R. H. Schindler, *California Institute of Technology*; K. O. Buddell, R. E. Cassell, D. H. Coward, K. F. Einswiler, D. P. Hutchinson, L. Moss, R. F. Mozley, A. Odian, J. R. Roebrig, W. Toki, Y. Uuno, F. Villa, N. Wetmes, and D. E. Wisinski, *Stanford Linear Accelerator Center*; H. L. Bledsoe, D. E. Dorfan, R. Fabrizio, F. Gracagnolo, R. P. Hamilton, C. A. Heusch, J. Perrier, H. F. Sadozinski, T. L. Schalk, A. Seiden, and D. B. Smith, *University of California at Santa Cruz*; J. J. Becker, G. T. Blaylock, H. Cui, B. Eisenstein, G. Gladding, S. A. Plaetzer, A. L. Spadasoro, J. J. Thaler, A. Wattenberg, and W. J. Wisinski, *University of Illinois, Champaign-Urbana*; J. S. Brown, T. H. Burnett, V. Cook, C. Del Papa, A. L. Duncan, P. M. Mockett, A. Nappi, J. C. Sleeman, and H. J. Willutzki, *University of Washington, Seattle*.

Presented at the 11th SLAC Summer Institute on Particle Physics  
Stanford, California, July 18-29, 1983

DE84 005326

## 1. Introduction

The SPEAR energy range, explored now for over a decade, has an enormous amount of physics remaining to be studied in both strong and weak interactions. Since the Crystal Ball and MARK II discoveries of new  $J/\psi$  radiative decays the area has become very topical in strong interaction physics. QCD suggests that  $J/\psi$ 's radiatively decay to two gluons and these gluons may form bound states or glueballs. This has generated a large amount of theoretical interest. In weak interactions, because the charged and neutral D lifetimes appear to be different, there has been considerable interest in understanding why the naive weak spectator models fail to explain this difference. Since MARK III will have a larger data sample than obtained by MARK II, there may be unexpected results, possibly as exciting as those in kaon physics. It may also prove as interesting to examine with large statistics are decays of  $\tau$ 's,  $F$ 's,  $\psi'$ 's, and  $A_c$ 's.

MARK III is a general purpose magnetic solenoidal detector that was installed in the West pit at SPEAR in July 1981. The initial checkout was completed in the fall of 1981 and the first data run was done at the  $J/\psi$  in the spring of 1982. This was followed in the fall of 1982 by running at the  $\psi''$ . In the spring of 1983 the first half of the running was again devoted to running at the  $J/\psi$ , accumulating a total (1982+1983) of  $2.7 \times 10^6$  produced  $J/\psi$  decays. During the second half a run at the  $\psi''$  allowed the accumulation of a total (1982+1983) integrated luminosity of  $\sim 5800 \text{ nb}^{-1}$  or  $\sim 45,000$  produced  $D\bar{D}$  pairs.

This report will describe the detector hardware, the performance of the detector on known  $J/\psi$  decays, and will finally discuss new results on  $\eta_c$  decays and radiative  $J/\psi$  decays. The results being presented are preliminary and are based on analyses completed in July 1983.

## 2. Apparatus

The MARK III detector has been designed to study  $e^+e^-$  reactions produced at SPEAR.<sup>1</sup> The detector is shown in the transverse and axial views in Figs. 1 and 2. The main design goals were to achieve large acceptance for charged and

MASTER

## DISCLAIMER

This report was prepared as an account of work sponsored by an agency of the United States Government. Neither the United States Government nor any agency thereof, nor any of their employees, makes any warranty, express or implied, or assumes any legal liability or responsibility for the accuracy, completeness, or usefulness of any information, apparatus, product, or process disclosed, or represents that its use would not infringe privately owned rights. Reference herein to any specific commercial product, process, or service by trade name, trademark, manufacturer, or otherwise does not necessarily constitute or imply its endorsement, recommendation, or favoring by the United States Government or any agency thereof. The views and opinions of authors expressed herein do not necessarily state or reflect those of the United States Government or any agency thereof.

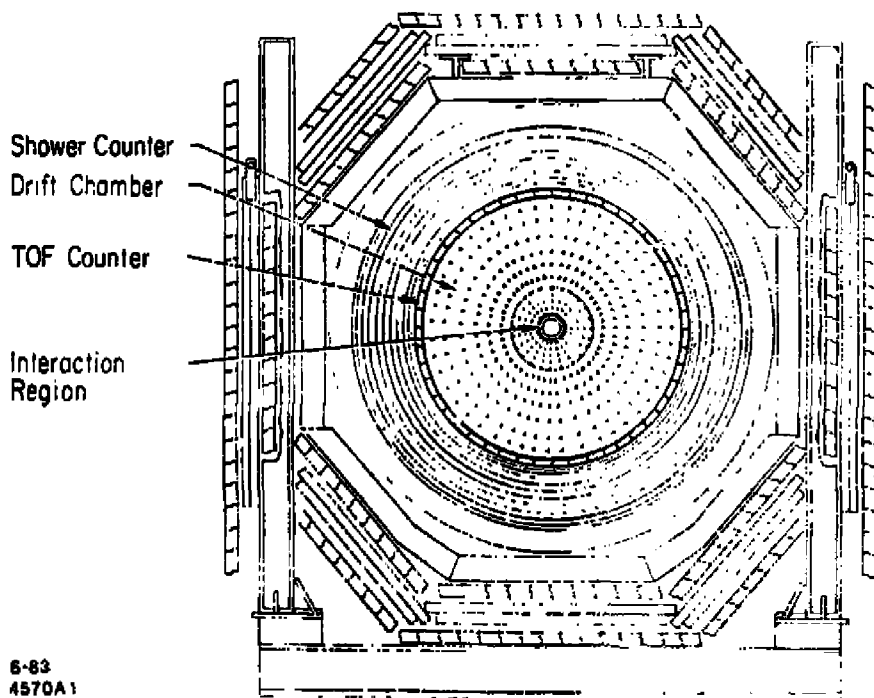
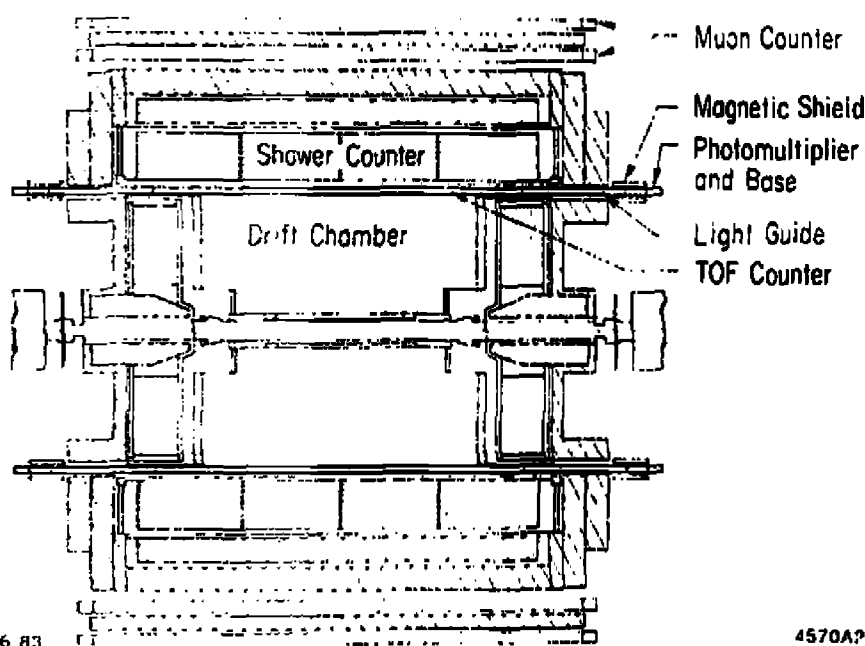


Fig. 1. Axial view of the MARK III detector.



6 83

4570A?

Fig. 2. Transverse view of the MARK III detector.

neutral particles, high detection efficiency for low energy gammas, good  $\pi/K/p$  separation by TOF and fine charged track momentum resolution. The typical events have relatively low multiplicities and charged particle momenta of several hundred MeV.

The description of the detector will begin with the central section of the drift chamber. The beam pipe and inner detectors were designed to minimize multiple scattering. The Beryllium beam pipe is 0.4% r.l. thick, the first inner drift chamber is constructed of Aluminum covered foam shells and the inner face of the main drift chamber is phenolic clad paper hexcell covered with Al foil. The main function of the inner drift chamber is to provide a pre-trigger. It has 4 layers with 32 axial sense wires per layer which are staggered by half a cell from layer to layer. The drift times in alternate sense wires in adjacent layers provide a time sum signal. This is fed into a chronotron circuit which is gated on SPEAR beam crossings to reduce the cosmic ray background and to provide a low pre-trigger rate of 3-4 kHz from the raw beam crossing rate of 1.28 mhz.

The second section of the drift chamber has 12 axial staggered sense wires in 32 cells which are read out both in time and charge. The high density of sense wires is useful for  $dE/dx$  sampling and Vee reconstruction for  $K_S$  and  $A$  decays. The  $dE/dx$  information was not used for the  $J/\psi$  analysis presented in this talk.

The third section of the drift chamber<sup>2</sup> has 4 axial and 2 stereo layers. Three of the axial layers include charge division. The basic cell design has 3 sense wires, two guard wires and five high voltage field shaping wires. This cell structure is repeated from 48 times in the 3rd layer to 128 times in the 8th layer. The drift chamber solid angle coverage is 85% of  $4\pi$  and the overall momentum resolution as measured on  $\mu$ -pairs in the  $J/\psi$  data is  $\sigma_p/p = 1.5\% \times \sqrt{1+p^2}$ ,  $p$  in GeV.

The TOF system<sup>3</sup> has 48 scintillators which are strapped on the exterior of the drift chamber. Each scintillator is read out by two phototubes through lucite lightguides. The radial distance is 1.17 m and the solid angle coverage is 80% of  $4\pi$ . The thick scintillator (5 cm) and the special design of the light guide enable high TOF resolution. The overall resolution ( $\sigma_{tof}$ ) is 175 ps for Bhabhas ( $J/\psi \rightarrow e^+e^-$ ), 168 ps for  $\mu$ -pairs ( $J/\psi \rightarrow \mu^+\mu^-$ ), and 189 ps for  $\pi$ 's

from  $J/\psi \rightarrow \rho\pi$  decays. The  $\pi/K/p$  separation is displayed in a  $\beta$  vs momentum scatter plot in Fig. 3.

The shower counter system consists of a barrel<sup>4</sup> and two endcaps.<sup>5</sup> The entire system is placed *inside* the magnet coil to improve the low energy gamma detection efficiency. The total angular coverage is 94% of  $4\pi$ . The shower counter is a gas proportional tube lead sandwich system with a single anode wire in a grounded cathode cell. Each anode wire is a high resistance stainless steel wire which is read out with an ADC on each end to measure energy deposition and position along the wire. The energy resolution on electrons is  $\sigma_E/E = 17\%/\sqrt{E}$ ,  $E$  in GeV, the  $\phi$  angular resolution ( $\sigma$ ) is 6 mrad on Bhabhas and the position resolution ( $\sigma$ ) per cell is 1% of the full wire length (337 cm).

Muon tubes mounted parallel to the beam axis (z-axis) on the exterior of the magnet cover 64% of  $4\pi$ . They are composed of two double sets of proportional tubes separated by 12.5 cm of steel plate. The  $\phi$  position of the track is determined by hits in two overlapping tubes and the z-position by charge division on the stainless steel anode wire. The resolution in z is 1% of the full wire length. The muon tube position resolution is limited by multiple scattering in the magnet steel.

The trigger system<sup>6</sup> utilizes hit patterns in layers 1, 3 and 5 to define drift chamber tracks. The number of drift chamber tracks required to trigger is selectable by computer control. The actual data taking trigger required 1 drift chamber track and 1 TOF hit, or 2 drift chamber tracks. The event rate at the  $J/\psi$  was  $\sim 3$  Hz and the real hadronic rate was slightly less than 1 Hz.

### 3. Performance Checks

The detector is studied with a variety of well known  $J/\psi$  decays. The basic analysis technique is to kinematically fit events using the four constraints of energy and momentum conservation (4-C fit). Kinematic fitting substantially improves the energy resolution for the  $\gamma$ 's, and has been successfully applied to events with up to five  $\gamma$ 's and four charged tracks. If the decay includes a  $\pi^0$  or

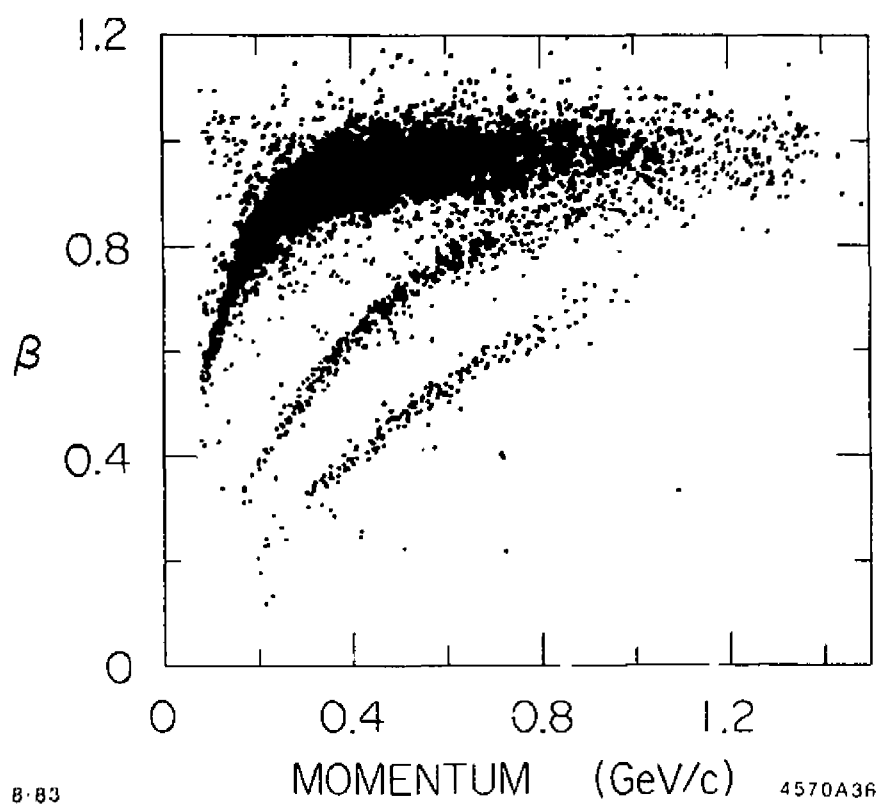


Fig. 3. Scatter plot of  $\beta$  versus momentum (GeV).

an  $\eta$ , then an additional mass constraint can be applied to the  $\gamma\gamma$  system (5-C). One difficulty is the presence of spurious photons, which are due to hadronic interactions of charged particles in the shower counter. These can be removed by ignoring showers near charged tracks. TOF identification is required when topologies include kaons or protons.

The reaction  $J/\psi \rightarrow \pi^+ \pi^- \pi^0$  is studied with high statistics. The events are subjected to a 4-C fit to the hypothesis  $J/\psi \rightarrow \gamma\gamma\pi^+ \pi^-$  resulting in 22k events. A typical event is shown in Fig. 4. The Dalitz plot in Fig. 5 shows clear  $\rho^0\pi^0$ ,  $\rho^+\pi^-$ , and  $\rho^-\pi^+$  bands. The charged and neutral  $\rho$  mass plots are shown in Figs. 6(a), (b) and (c). The efficiency determined from a Monte Carlo simulation is 48%. The observed branching ratio,  $\text{BR}(J/\psi \rightarrow \pi^+ \pi^- \pi^0) = (1.49 \pm 22) \times 10^{-2}$ , is in agreement with Particle Data Table<sup>7</sup> values. The ratio of the  $\rho\pi$  rates is  $\text{BR}(J/\psi \rightarrow \rho^0\pi^0) / \text{BR}(J/\psi \rightarrow \rho^\pm\pi^\mp) = .498 \pm .04$ , which is expected if the  $J/\psi$  has isospin 0.

The reaction  $J/\psi \rightarrow \rho^0\pi^0$  is very useful to study the shower counter  $\gamma$  detection efficiency and the  $\gamma\gamma$  mass resolution. The  $\pi^0$  from this decay is produced essentially monochromatically at 1.45 GeV, and the  $\gamma$ 's from these decays have an energy spectrum in the LAB frame that is flat from nearly 0 to 1.45 GeV. The energy spectrum (LAB) and  $\cos\theta_\gamma$  ( $\pi^0$  CMS) are plotted in Fig. 7. The angular distribution is flat as expected for spin 0 decays except at  $\cos\theta_\gamma = \pm 1$ . Those two regions correspond to the  $\gamma$ 's moving parallel and antiparallel to the  $\pi^0$  direction. In the LAB frame the forward going  $\gamma$  has most of the  $\pi^0$  momentum whereas the other  $\gamma$  has very low momentum. The energy distribution is flat to 100 MeV and falls to 50% at 50 MeV. This decay also allows a study of the  $\gamma\gamma$  mass resolution. Figs. 8(a) and (b) are the reconstructed masses of the  $\pi^0$  using the 4-C fitted energies and raw shower energies respectively. The mass resolution is a factor of three better with the 4-C fitted energies than with the raw shower energies.

The decay  $J/\psi \rightarrow \gamma\eta'$  is studied in two decay modes,  $\eta' \rightarrow \gamma\rho^0$  and  $\eta' \rightarrow \eta\pi^+\pi^-$  ( $\eta \rightarrow \gamma\gamma$ ). In the first mode a 4-C kinematic fit to  $J/\psi \rightarrow \gamma\gamma\pi^+\pi^-$  is applied. Further cuts of  $\text{mass}(\gamma\gamma) > 200$  MeV, to remove  $\rho\pi$  background, and  $.425 < \text{mass}(\pi^+\pi^-) < .925$  MeV, to select events with  $\rho^0$ 's, are applied. The re-

Fitted  $\psi \rightarrow \pi^+ \pi^- \pi^0$  Event

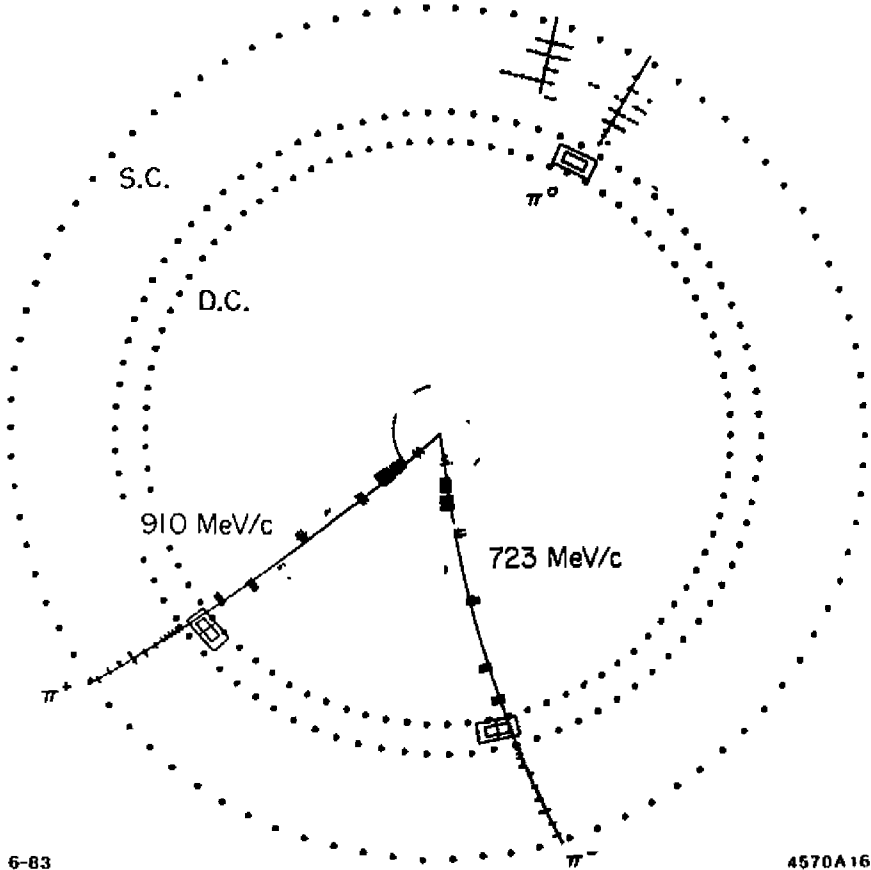


Fig. 4.  $J/\psi \rightarrow \pi^+ \pi^- \pi^0$  event display.

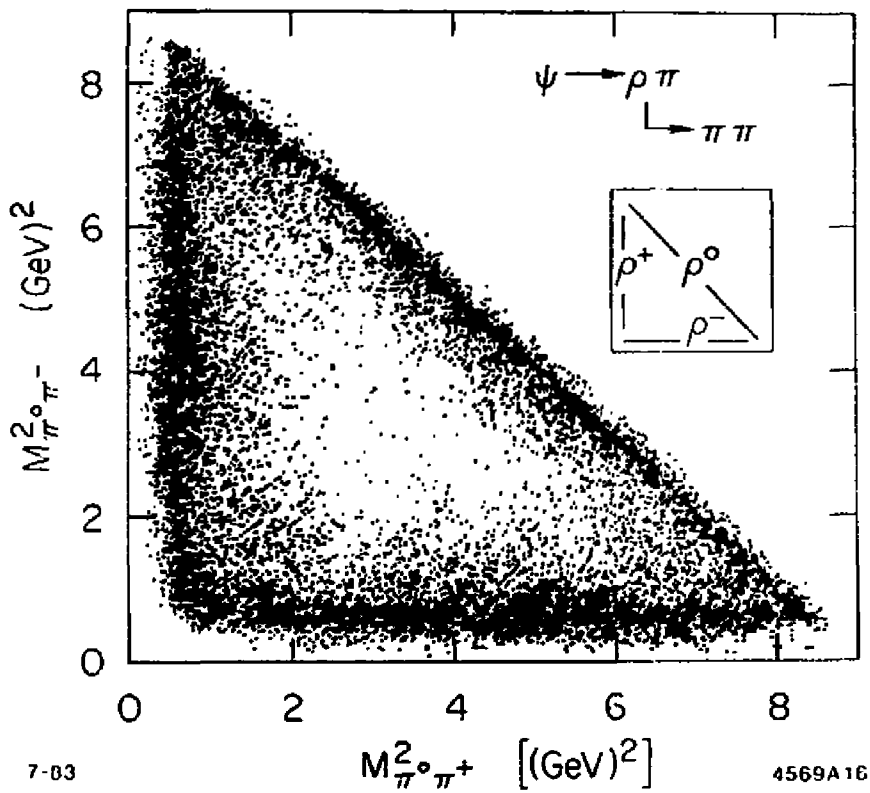


Fig. 5. Dalitz plot  $mass_{\pi^+\pi^0}^2$  versus  $mass_{\pi^-\pi^0}^2$  from  $J/\psi \rightarrow \pi^+\pi^-\pi^0$ . The schematic drawing displays the bands of the  $\rho$  decay modes.

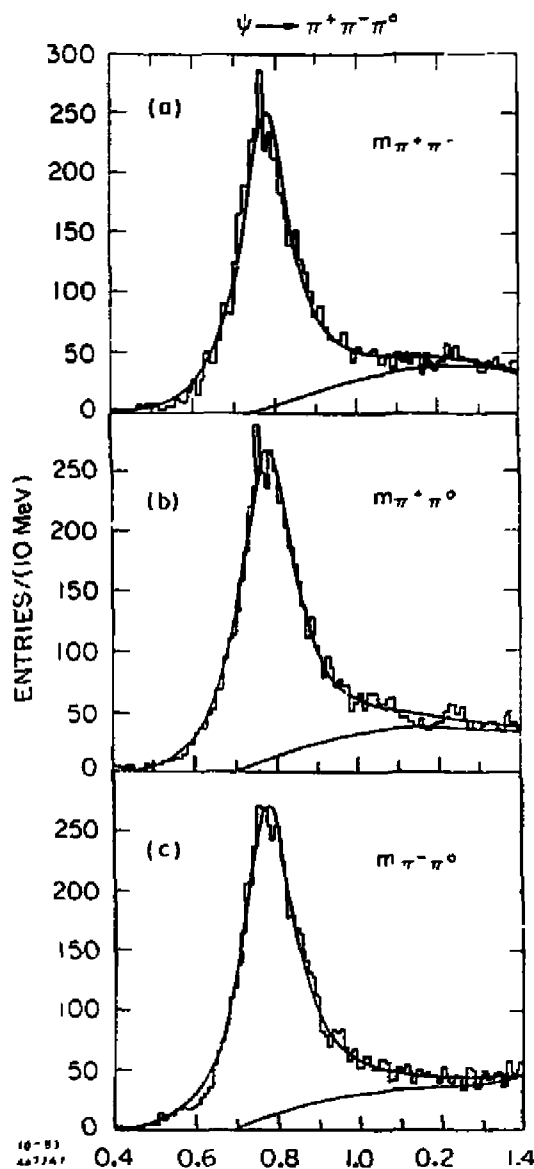


Fig. 6. (a)  $Mass_{\pi^+ \pi^-}$  (GeV) distribution from  $J/\psi \rightarrow \pi^+ \pi^- \pi^0$ , drawn with a fit of a Breit-Wigner curve. (b)  $Mass_{\pi^+ \pi^0}$  (GeV) distribution from  $J/\psi \rightarrow \pi^+ \pi^- \pi^0$ , drawn with a fit of a Breit-Wigner curve. (c)  $Mass_{\pi^+ \pi^0}$  (GeV) distribution from  $J/\psi \rightarrow \pi^+ \pi^- \pi^0$  drawn with a fit of a Breit-Wigner curve.

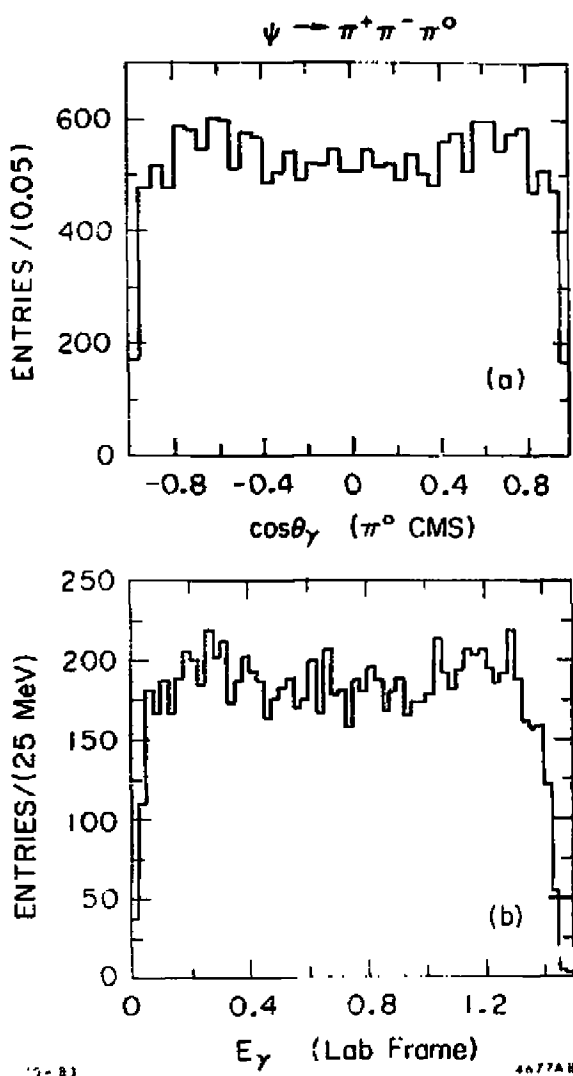


Fig. 7. (a)  $\cos\theta_\gamma$  distribution in the  $\pi^0$  CMS from  $J/\psi \rightarrow \rho^0 \pi^0$ . (b)  $\gamma$  energy (GeV) distribution in the LAB frame from the 1.45 GeV  $\pi^0$  from  $J/\psi \rightarrow \rho^0 \pi^0$ .

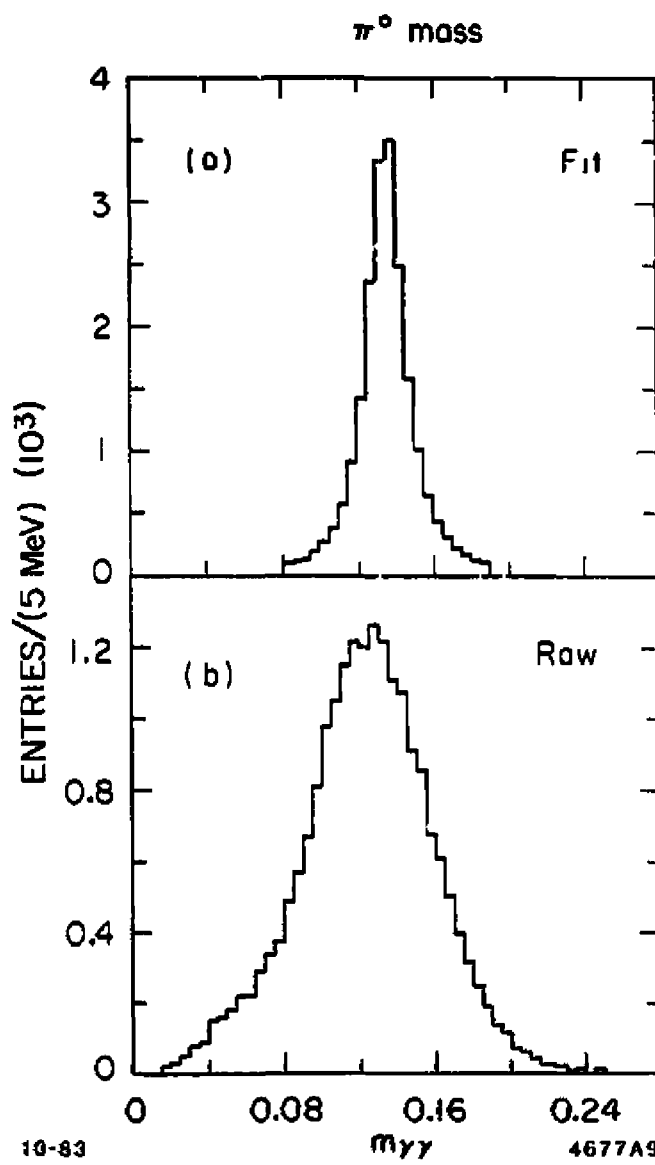


Fig. 8. (a) Reconstructed  $\pi^0$  mass distribution using 4-C fitted  $\gamma$  energies. (b) Reconstructed  $\pi^0$  mass distribution using raw shower counter energies.

resulting  $\gamma\pi^+\pi^-$  mass distribution is shown in Fig. 9(a). The fitted mean is  $957 \pm 5$  MeV and the mass resolution ( $\sigma$ ) is  $9 \pm 4$  MeV. In the second decay mode a kinematic 4-C fit to  $J/\psi \rightarrow \gamma\gamma\pi^+\pi^-$  and a 5-C fit to  $J/\psi \rightarrow \gamma\eta\pi^+\pi^-$  are applied. The resulting mass( $\gamma\eta\pi^+\pi^-$ ) distribution from the 5-C fits is shown in Fig. 9(b). The mean mass is  $958 \pm 3$  MeV and the mass resolution ( $\sigma$ ) is 5.7 MeV. The branching ratio is  $\text{BR}(J/\psi \rightarrow \gamma\eta') = (4.6 \pm 4.2\text{statistical}) \pm 8.5\text{systematic}) \times 10^{-3}$ . Both branching ratios are in reasonable agreement with the Particle Data Table<sup>8</sup> value of  $\text{BR}(J/\psi \rightarrow \gamma\eta') = (3.6 \pm 0.5) \times 10^{-3}$ .

These results demonstrate that the MARK III detector performs very well detecting and reconstructing radiative decays. The efficiency for low energy  $\gamma$  detection is very high. The mass resolution ( $\sigma$ ) achieved with constraint fitting is 8 MeV for  $\pi^0$ 's in  $\rho\pi$  decays, 9 MeV for the  $\eta'$  in the  $\gamma\rho$  mode and 5.7 MeV in the  $\eta\pi^+\pi^-$  mode. The mass scale agrees to within 1 MeV with nominal values. The measured branching ratios agree with published values, showing that the luminosity and the Monte Carlo simulation are understood.

#### 4. $\eta_c$ Results

##### Experimental Situation

The Crystal Ball experiment at SPEAR first observed the  $\eta_c$  in the inclusive  $\gamma$  spectrum in  $J/\psi$  and  $\psi'$  decays,<sup>9</sup> and obtained the following results,

$$m = 2984 \pm 4 \text{ MeV}$$

$$\Gamma = 12.4 \pm 4.1 \text{ MeV}$$

$$\text{BR}(J/\psi \rightarrow \gamma\eta_c) = (1.27 \pm 3.0) \times 10^{-2}$$

The observed hadronic modes of the  $\eta_c$  have been rather sparse. In the  $J/\psi$  radiative decays, where the radiative  $\gamma$  energy is low ( $E_\gamma = 112$  MeV), the Crystal Ball<sup>10</sup> observed  $18 \pm 6$  events in the mode  $\eta_c \rightarrow \eta\pi^+\pi^-$ . In the  $\psi'$  radiative decays, the MARK II observed 3 events in the mode  $\eta_c \rightarrow p\bar{p}$ , 8 events in the mode  $\eta_c \rightarrow \pi^\pm K^\mp K_S$  and by combining these modes with other hadronic modes a signal of about 25 events was obtained.<sup>11</sup> There has been no spin-parity determination for the  $\eta_c$ .

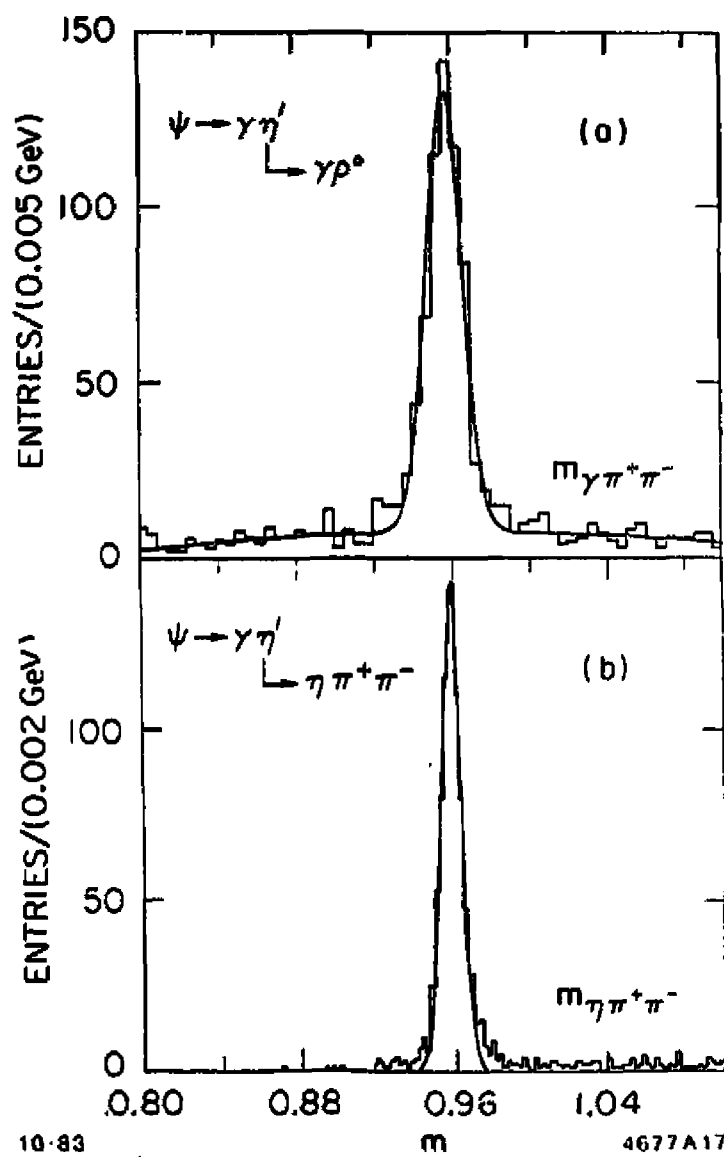


Fig. 9. (a)  $Mass_{\gamma \rho^0}$  (GeV) distribution from  $J/\psi \rightarrow \gamma \rho^0$ . (b)  $Mass_{\eta \pi^+ \pi^-}$  (GeV) distribution from  $J/\psi \rightarrow \gamma \eta \pi^+ \pi^-$ .

## MARK III Results

Three  $\eta_c$  decay modes from  $J/\psi$  radiative decays will be presented,  $J/\psi \rightarrow \eta p\bar{p}$ ,  $J/\psi \rightarrow \eta\eta\pi^+\pi^-$ , and  $J/\psi \rightarrow \eta\phi\phi$ . Other modes will appear in future publications.

In the  $p\bar{p}$  mode the analysis requires TOF identification followed by 4-C fits to the hypotheses  $J/\psi \rightarrow \gamma p\bar{p}$  and  $J/\psi \rightarrow \gamma\gamma p\bar{p}$ . To remove spurious  $\gamma$ 's caused by hadronic interactions of the charged tracks in the shower counter,  $\gamma$ 's close to the  $p$ 's and  $\bar{p}$ 's are excluded. Often the  $p$ 's annihilate and produce a large amount of background. Figure 10 is a typical event of  $J/\psi \rightarrow \eta p\bar{p}$ . An important background is  $J/\psi \rightarrow \pi^0 p\bar{p}$ . This is removed by excluding events that fit to  $J/\psi \rightarrow \gamma\gamma p\bar{p}$  with  $m_{\gamma\gamma} \approx m_{\pi^0}$ . After these preliminary cuts the  $\eta_c$  signal appears just below a large feed through of  $J/\psi \rightarrow p\bar{p}$ . This background is removed with a collinearity cut between the  $p$  and the  $\bar{p}$ . The resulting mass plot is shown in Fig. 11. The branching ratio obtained is  $BR(J/\psi \rightarrow \gamma\eta_c) \times BR(\eta_c \rightarrow p\bar{p}) = (2.2 \pm .6 \pm .5) \times 10^{-6}$ . Using the Crystal Ball inclusive rate,  $BR(J/\psi \rightarrow \gamma\eta_c) = (1.27 \pm .36) \times 10^{-5}$ , the  $\eta_c$  branching ratio becomes  $BR(\eta_c \rightarrow p\bar{p}) = (.18 \pm .09) \times 10^{-2}$ . This is very close to the rate observed for the direct decay  $J/\psi \rightarrow p\bar{p}$ .<sup>12</sup>

The mode  $\eta_c \rightarrow \eta\pi^+\pi^-$  is observed with a large signal. The events are fit to  $J/\psi \rightarrow \gamma\gamma\eta\pi^+\pi^-$  and  $J/\psi \rightarrow \gamma\eta\pi^+\pi^-$ . The  $mass(\eta\pi^+\pi^-)$  distribution is shown in Fig. 12. The fitted mass is  $2.967 \pm 0.004(\text{fit}) \pm 0.01(\text{systematic})$  MeV. The mass resolution ( $\sigma$ ) is 20 MeV, which is consistent with the detector resolution as determined by Monte Carlo simulation. The measured branching ratio is  $BR(J/\psi \rightarrow \gamma\eta_c) \times BR(\eta_c \rightarrow \eta\pi^+\pi^-) = [4.3 \pm .7(\text{stat}) \pm 1.3(\text{syst})] \times 10^{-4}$ .

The mode  $\eta_c \rightarrow \phi\phi$  is observed via the  $\phi$  decay to  $K^+K^-$ . Figure 13 shows a typical event. The initial data selection required 4 charged prongs with total charge zero and TOF identification for at least one  $K$  in each oppositely charged pair. After requiring that there is one  $\phi$ , it is seen that the other recoiling  $K^+K^-$  pair also forms a  $\phi$  as shown in Fig. 14(a). Requiring that both  $K^+K^-$  pairs are  $\phi$ 's and then looking at the quantity  $E_{miss}$  (missing energy from the two  $\phi$ 's)- $P_{miss}$  (missing momentum from the two  $\phi$ 's) as shown in Fig. 14(b), it is

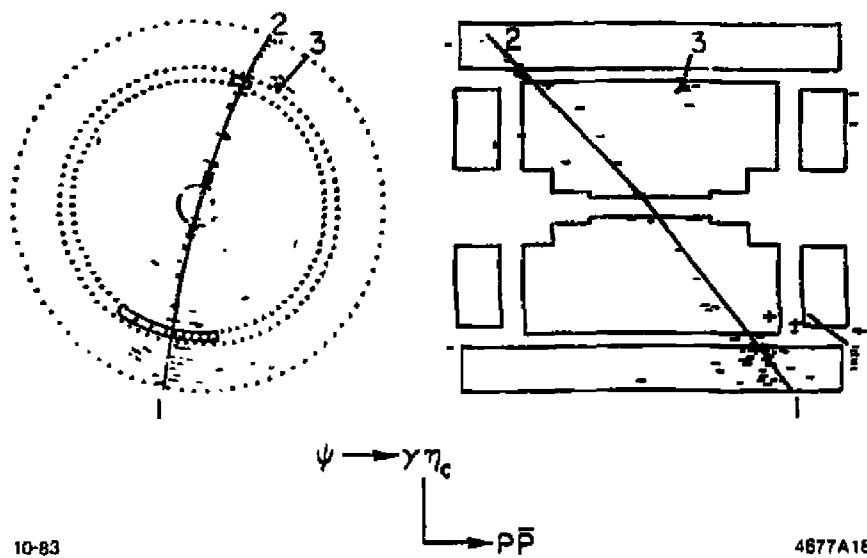


Fig. 10.  $J/\psi \rightarrow \gamma \eta_c$  event display.

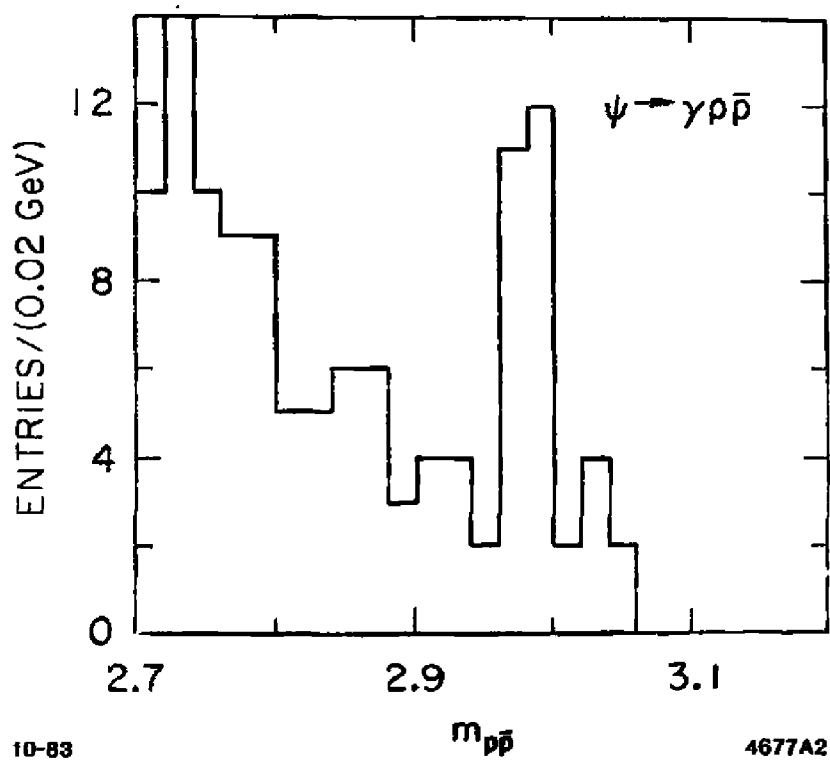


Fig. 11.  $Mass_{p\bar{p}}$  (GeV) distribution after the collinearity cut from  $J/\psi \rightarrow \gamma p\bar{p}$ .

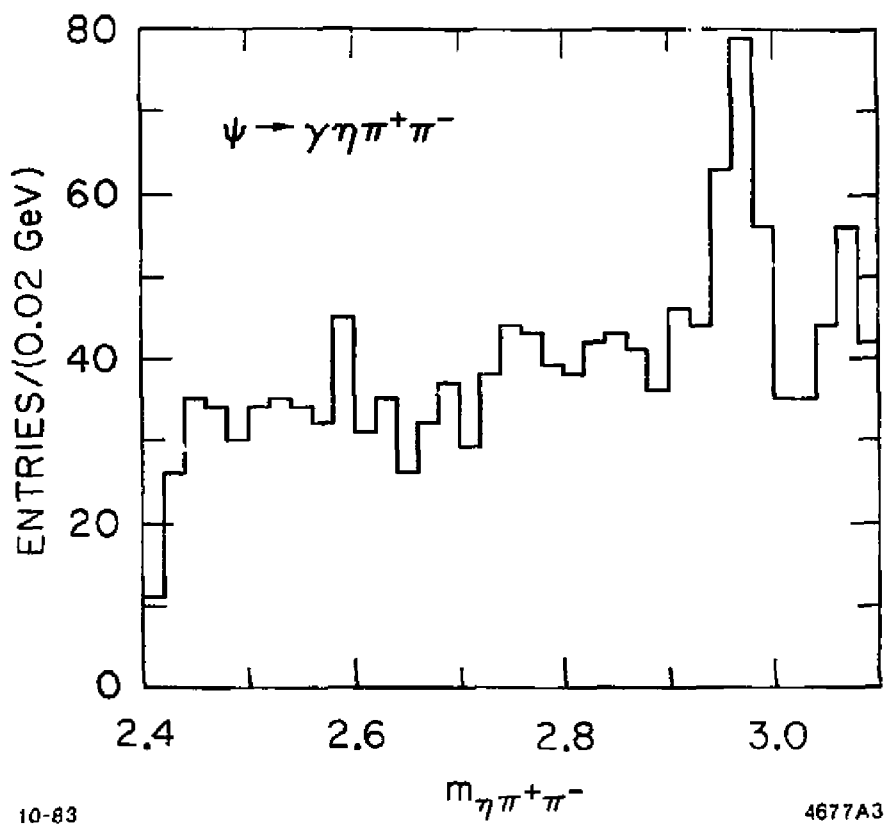


Fig. 12.  $Mass_{\eta\pi^+\pi^-}$  (GeV) distribution from  $J/\psi \rightarrow \gamma\eta\pi^+\pi^-$ .

$\psi - \gamma\phi\phi$  Event

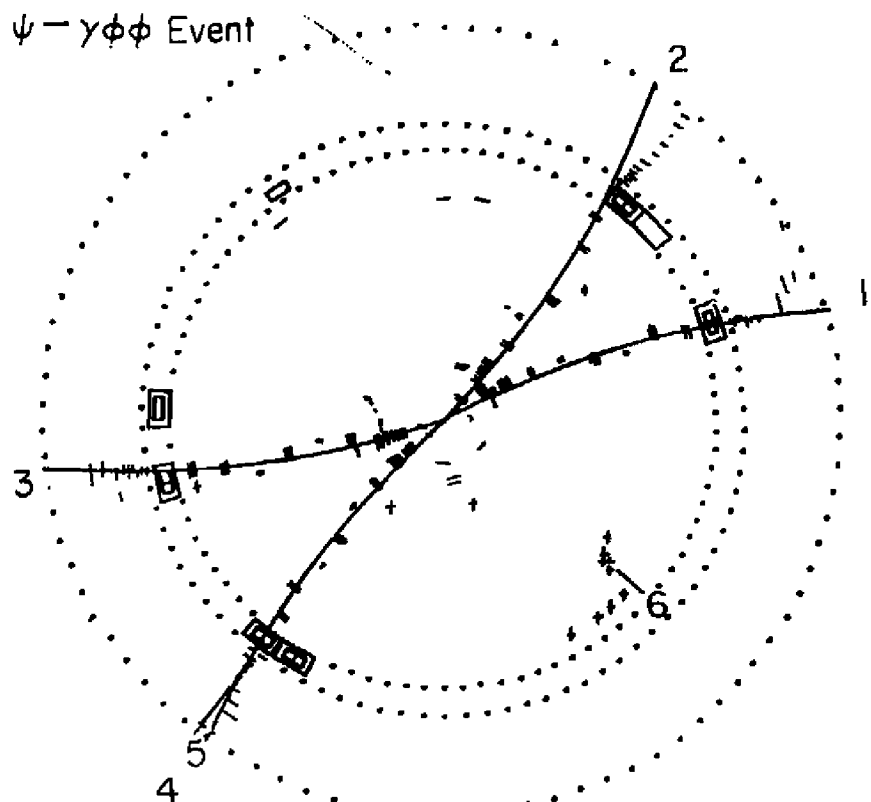


Fig. 13.  $J/\psi \rightarrow \gamma\phi\phi$  event display.

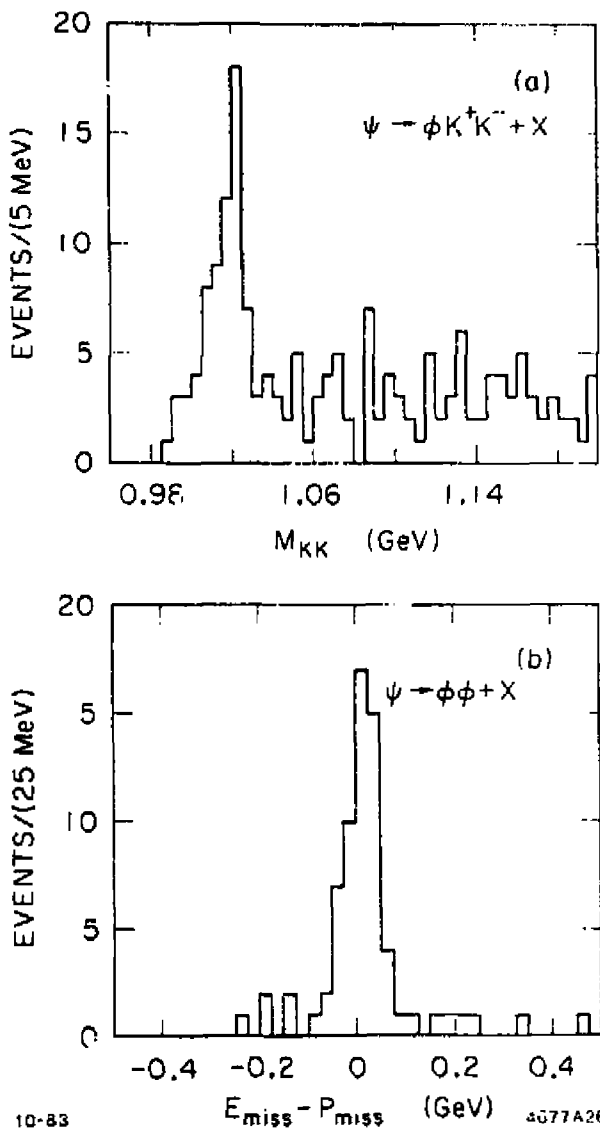


Fig. 14. (a)  $M_{K^+K^-}$  (GeV) distribution recoiling against a  $\phi$ . (b)  $E_{miss} - P_{miss}$  (GeV) from the  $\phi\phi$ .

seen that the recoiling mass against the  $\phi\phi$  system could only be a  $\gamma$ . It should be noted that neither  $J/\psi \rightarrow \pi^0\phi\phi$  nor  $J/\psi \rightarrow \phi\phi$  is allowed by charge conjugation invariance. The events are 4-C fit to  $J/\psi \rightarrow \gamma K^+K^-K^+K^-$  and the resulting  $\phi\phi$  mass is shown in Fig. 15. A clear signal is observed at the  $\eta_c$  mass. The efficiency of detecting  $J/\psi \rightarrow \gamma\phi\phi$  as a function of  $\phi\phi$  mass is also shown in Fig. 15. The branching ratio for the  $\eta_c$  is  $BR(J/\psi \rightarrow \gamma\eta_c) \times BR(\eta_c \rightarrow \phi\phi) = (1.24 \pm .32) \times 10^{-4}$ . The fitted mass is 2.078 GeV and its width is consistent with the detector resolution. Due to kaon decays, the efficiency rapidly decreases to a few percent in the mass region near 2 GeV. Therefore it is difficult to determine if there is any structure in the region near 2 GeV.

The decay angles in the  $\phi\phi$  mode allow a definitive  $\eta_c$  spin-parity determination.<sup>13-14</sup> This test is analogous to the  $\pi^0$  spin-parity analysis<sup>15</sup> from the reaction  $\pi^0 \rightarrow e^+e^-e^+e^-$ . The useful decay angles (actually there are seven) are  $\Theta_\gamma$ , the angle between the radiative  $\gamma$  and the  $e^+e^-$  beam direction in the LAB frame,  $\Theta_\phi$ , the angle between  $\gamma$ ,  $\eta_c$  and one  $\phi$  in the  $\eta_c$  CMS frame,  $\Theta_{K^+}$ , the angle between the  $\phi$  and the  $K^+$  in the  $\phi$  CMS frame, and  $\chi$ , the angle between the decay planes of the  $\phi$ 's in the  $\eta_c$  CMS frame. These decay angles are plotted in Figs. 16, 17, 18 and 19. The lines show what is expected for  $J^P=0^-$ . The angles  $\chi$  and  $\Theta_{K^+}$  are most sensitive for likelihood tests of  $J^P$  and are independent of the initial polarization of the  $\eta_c$ . The event distributions are proportional to  $1 + \beta \times \cos(2\chi)$  and  $1 + \varsigma \times P_2(\Theta_{K^+})$ , where  $\beta$  and  $\varsigma$  depend on the  $J^P$  and  $P_2$  is the Legendre polynomial. The likelihood ratios for different  $J^P$  relative to  $0^-$ , assuming lowest  $l$  values, are summarized in Table 1.

$J^P=0^-$  is preferred overall as expected. This is the first spin-parity determination of the  $\eta_c$ . A more complete analysis will include a simultaneous fit to all the decay angles.

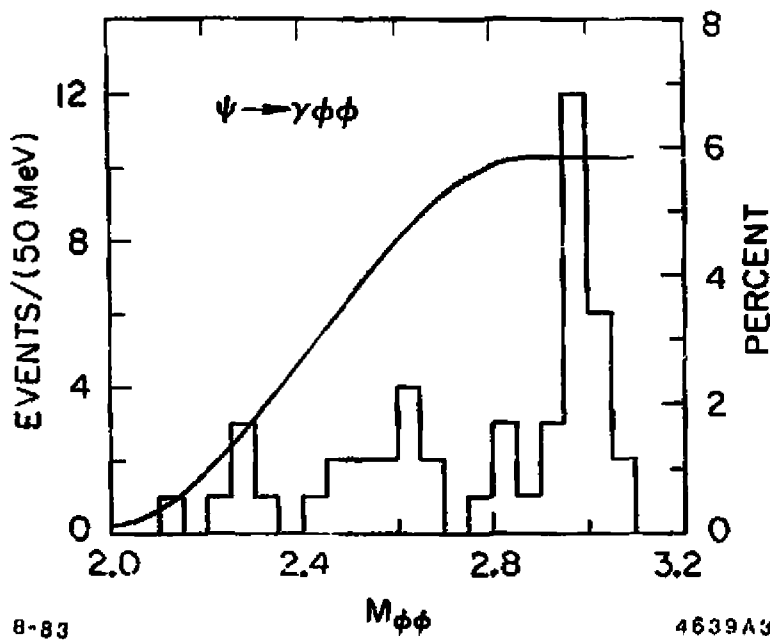


Fig. 15.  $M_{\phi\phi}$  (GeV) distribution from  $J/\psi \rightarrow \gamma\phi\phi$  with the mass acceptance overplotted.

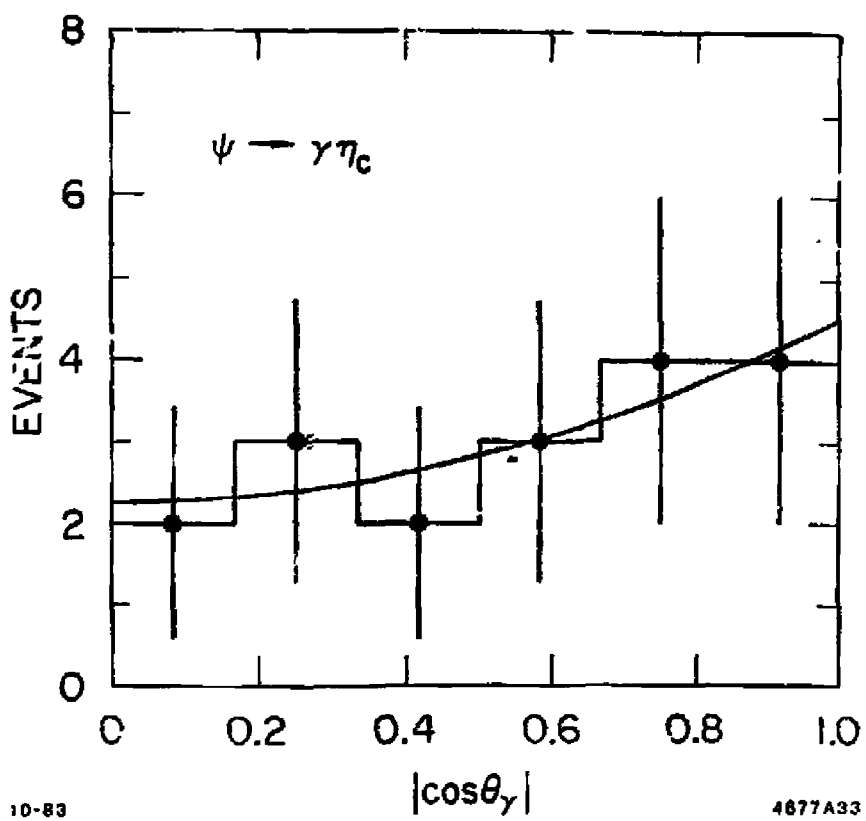
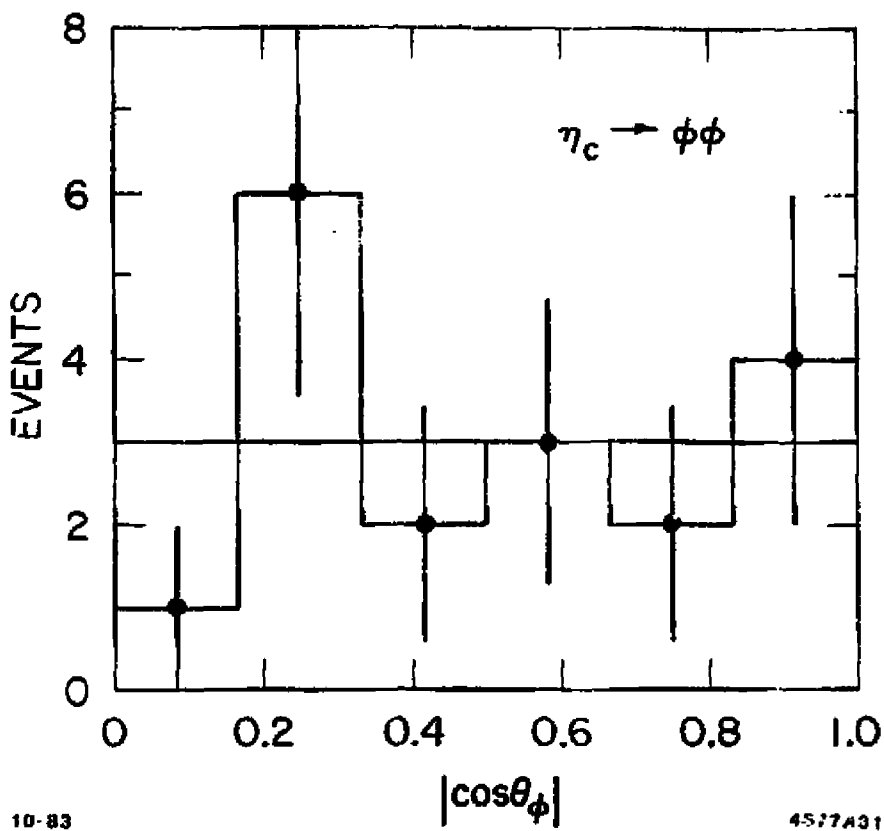


Fig. 16.  $\cos\theta_\gamma$  in  $J/\psi \rightarrow \gamma\eta\eta$  decays. The curve is the expected distribution for  $J^P=0^-$ .



10-83

4577431

Fig. 17.  $\cos\theta_\phi$  in  $J/\psi \rightarrow \gamma\phi\phi$  decays. The curve is the expected distribution for  $J^P = 0^-$ .

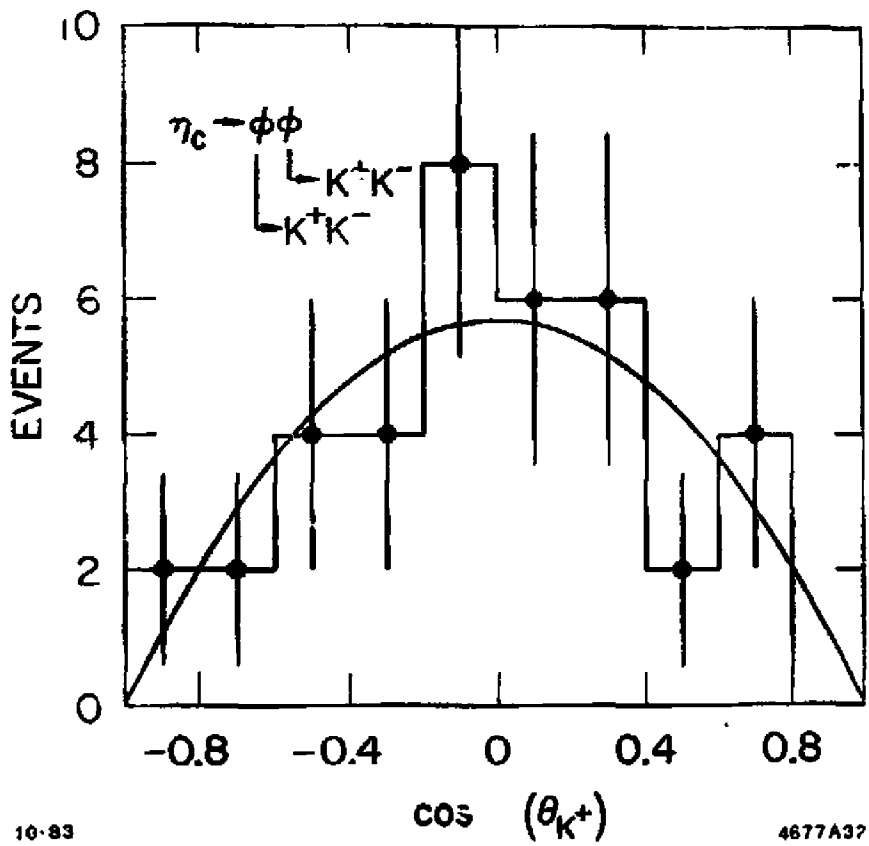
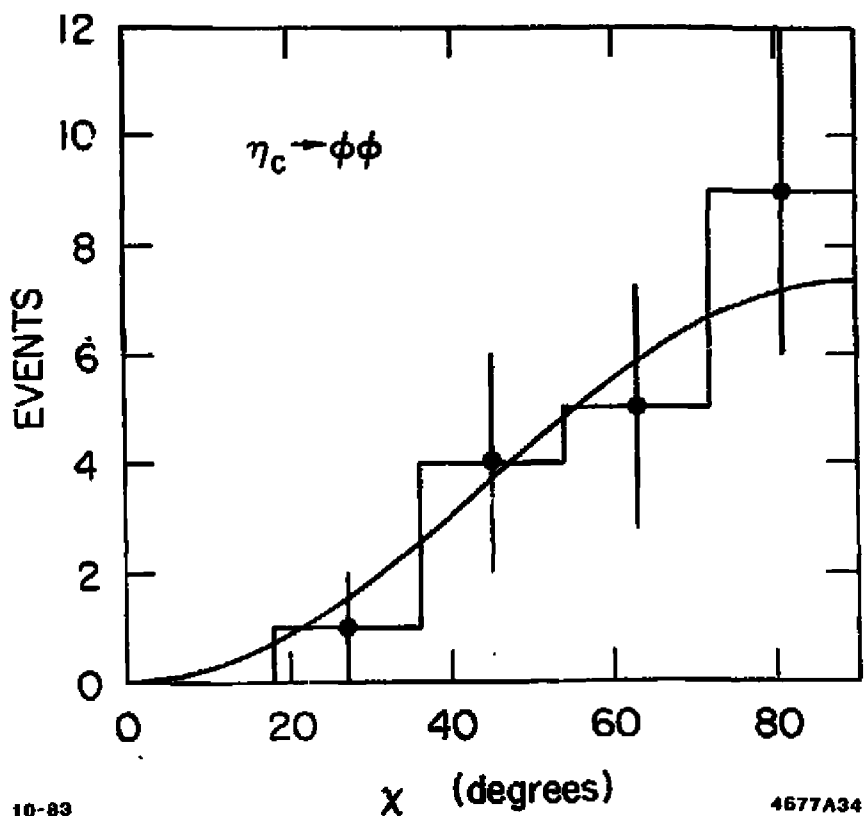


Fig. 18.  $\cos\theta_{K^+}$  in  $J/\psi \rightarrow \gamma \phi \phi$  decays. The curve is the expected distribution for  $J^P = 0^-$ .



10-83

4677A34

Fig. 19.  $\chi$  angle in  $J/\psi \rightarrow \gamma\phi\phi$  decays. The curve is the expected distribution for  $J^P = 0^-$ .

Table 1. Likelihood Ratios for  $\beta$  and  $\xi$  Tests

$J^P$	Likelihood Ratio of $0^-$ to $J^P$ for $\beta$	Likelihood Ratio of $0^-$ to $J^P$ for $\xi$
odd $^\pm$	1100	47
0 $^+$	$>10^5$	7.7
2 $^-$	36	5.7
2 $^+$	2400	7.7

### 5. $J/\psi$ Radiative Results

#### Physics Interest

Recently there has been much interest in  $J/\psi$  radiative decays. Quantum Chromodynamics allows the existence of bound states of gluons or glueballs and the  $J/\psi$  radiative decays appear to be an ideal place to look for such states.<sup>16</sup> QCD predicts a large branching ratio for radiative decays by comparing the calculated rates between  $J/\psi \rightarrow \gamma gg$  and  $J/\psi \rightarrow ggg$ .<sup>17-19</sup> The calculation predicts,

$$\Gamma(J/\psi \rightarrow \gamma + \text{hadrons})/\Gamma(J/\psi \rightarrow \text{hadrons}) \approx 10\%$$

The known measured decays total  $\sim 1\%$ . Consequently, if QCD is correct there should be a large number of  $J/\psi$  radiative decays via 2 gluons which have not yet been seen. If there are bound states of 2 gluons they should be isoscalar SU(3) singlets with even C-parity. There are many models that predict glueball masses in the 1-2 GeV region and it is possible that their widths are narrow. The mass spectrum may be very complicated due to mixing with other  $q\bar{q}$  states. There may also be more complex bound states of  $ggg$ .<sup>20-21</sup> or  $g\bar{q}q\bar{q}$ .<sup>22</sup> The thrust of this discussion is that any new states found in radiative  $J/\psi$  decays are of considerable interest.

### Experimental Situation

Recently observed states in radiative decays are  $\iota \rightarrow K\bar{K}\pi^{23-24}$ ,  $\Theta \rightarrow K\bar{K}^{25}$  and  $\eta\eta^{26}$  and structures near 1700 MeV in  $\eta\pi\pi^{27}$  and  $\rho^0\rho^0^{28}$ .

In the  $K\bar{K}\pi$  channel the iota has been observed to have a very large branching ratio and Crystal Ball determined that the iota decays mainly via  $\delta\pi$  and its spin-parity is  $0^-$ . Various mixing models have predicted that in analogy to  $\eta'$ , the iota should have a large  $\gamma\rho^0$  decay mode.

In the  $\eta\eta$  channel Crystal Ball first observed the  $\Theta$  but did not clearly separate the state from the  $f'(1515)$ . They did a maximum likelihood test on the spin-parity of the  $\Theta$  and found that  $J^P=2^+$  is favored over  $0^+$ . If the  $\Theta$  is a glueball there are predictions that it should be an SU(3) singlet and should decay to  $\pi\pi$ .

In the  $\eta\pi\pi$  channel Crystal Ball found a broad structure around 1.7 GeV but set a limit on  $\iota \rightarrow \eta\pi\pi$ . This may be in conflict with the previous observation that the iota decays to  $\delta\pi$ , because the  $\delta$  also decays to  $\eta\pi$ .

### MARK III Results

MARK III has studied a large number of radiative decays. The preliminary results on the following decays will be shown:  $J/\psi \rightarrow \gamma\pi^+\pi^-$ ,  $\gamma K^+K^-$ ,  $\gamma\pi^0K_SK_S$ ,  $\gamma\pi^\pm K^\mp K_S$ ,  $\gamma\pi^0K^+K^-$ ,  $\gamma\gamma\rho^0$ , and  $\gamma\eta\pi^+\pi^-$ .

The decay mode to  $\gamma\pi^+\pi^-$  is studied by applying a 4-C fits to  $J/\psi \rightarrow \gamma\pi^+\pi^-$  and removing  $\mu$ -pairs and radiative Bhabha ( $J/\psi \rightarrow \gamma e^+e^-$ ) events. The resulting mass( $\pi^+\pi^-$ ) distribution is shown in Fig. 20. The  $f(1270)$  is clearly seen and feed through of  $\rho\pi$  decays appears below 800 MeV. This feed through occurs when one of the two  $\gamma$ 's from the  $\pi^0$  in the  $\rho\pi$  decays is not detected and the reaction is incorrectly fitted to  $J/\psi \rightarrow \gamma\pi^+\pi^-$ . There are possible hints of structure above the  $f(1270)$  but further analysis is required to remove more background. The Dalitz plot in Fig. 21 shows the  $f(1270)$  band and the outline of the  $\rho\pi$  feed through. The  $f(1270)$  peak is fitted with a nonrelativistic Breit-

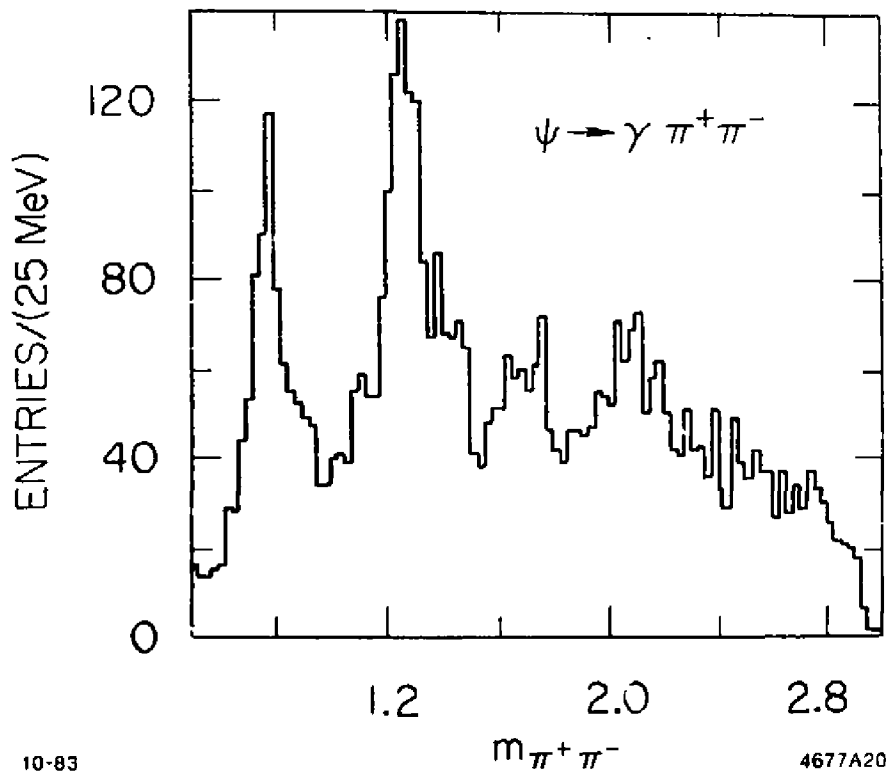


Fig. 20.  $Mass_{\pi^+\pi^-}$  (GeV) distribution from  $J/\psi \rightarrow \gamma \pi^+ \pi^-$ .

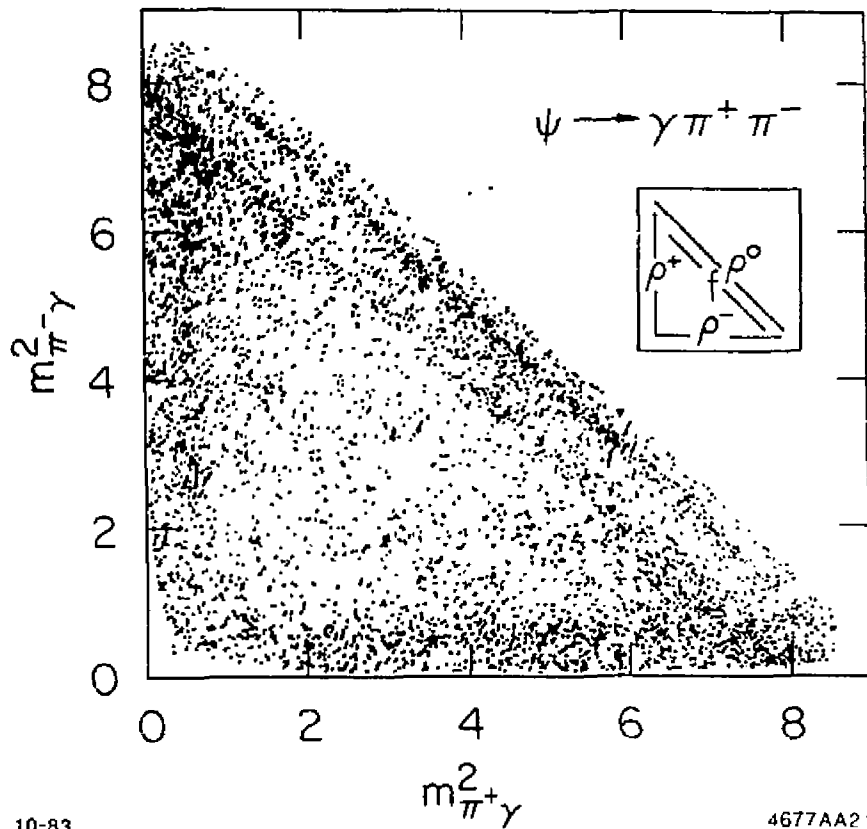


Fig. 21. Dalitz plot  $mass_{\pi^+\gamma}^2$  versus  $mass_{\pi^-\gamma}^2$  from  $J/\psi \rightarrow \gamma \pi^+ \pi^-$ . The schematic drawing displays the bands of the  $f$  decay and the  $\rho$  background.

Wigner curve and the measured values are,

$$m = 1278 \pm 5 \text{ MeV}$$

$$\Gamma = 155 \pm 15 \text{ MeV}$$

These are in agreement with Particle Data Table<sup>29</sup> values.

The decay mode  $J/\psi \rightarrow \gamma K^+ K^-$  is obtained by requiring 4-C fits and TOF identification. The mass( $K^+ K^-$ ) distribution is shown in Fig. 22. The  $\Theta$  and  $f'(1515)$  are clearly separated and there is evidence for a new state at 2.2 GeV which hereafter will be named the  $\xi$ . The new state has a 7 standard deviation significance. The Dalitz plot shown in Fig. 23 shows diagonal bands corresponding to the three states. The states are also observed in the mode  $J/\psi \rightarrow \gamma K_S K_S$  with lower statistics. Incoherent Breit-Wigner curves are simultaneously fit to the  $f'(1515)$ , the  $\Theta$ , and the new state, the  $\xi$ . In the fit the masses and the widths of the  $\theta$  and the  $\xi$  are allowed to vary but those of the  $f'(1515)$  are held fixed. The results are,

$$m_\Theta = 1.719 \pm 6 \text{ GeV}$$

$$\Gamma_\Theta = .117 \pm 23 \text{ GeV}$$

$$m_\xi = 2.22 \pm .015(\text{stat}) \pm .02(\text{sys}) \text{ GeV}$$

$$\Gamma_\xi = .03 \pm .015(\text{stat}) \pm .02(\text{sys}) \text{ GeV}$$

The mass plot with the fitted curves is shown in Fig. 24. The  $\xi$  width appears to be narrow in the  $K^+ K^-$  mode. To accurately determine the width, the detector resolution is being examined in both the  $K^+ K^-$  and the  $K_S K_S$  decay modes. The branching ratios are,

$$\text{BR}(J/\psi \rightarrow \gamma f') \times \text{BR}(f' \rightarrow K^+ K^-) = (1.6 \pm .3(\text{stat}) \pm .35(\text{sys})) \times 10^{-4}$$

$$\text{BR}(J/\psi \rightarrow \gamma \Theta) \times \text{BR}(\Theta \rightarrow K^+ K^-) = (4.8 \pm .7(\text{stat}) \pm .9(\text{sys})) \times 10^{-4}$$

$$\text{BR}(J/\psi \rightarrow \gamma \xi) \times \text{BR}(\xi \rightarrow K^+ K^-) = (8.0 \pm 2.0(\text{stat}) \pm 1.0(\text{sys})) \times 10^{-5}$$

The  $\xi$  is observed in three modes,  $\pi^0 K^+ K^-$ ,  $\pi^\pm K^\mp K_S$ , and for the first time  $\pi^\pm K^\mp K_S$ . The mass plots are shown in Figs. 25(a), (b) and (c). Using

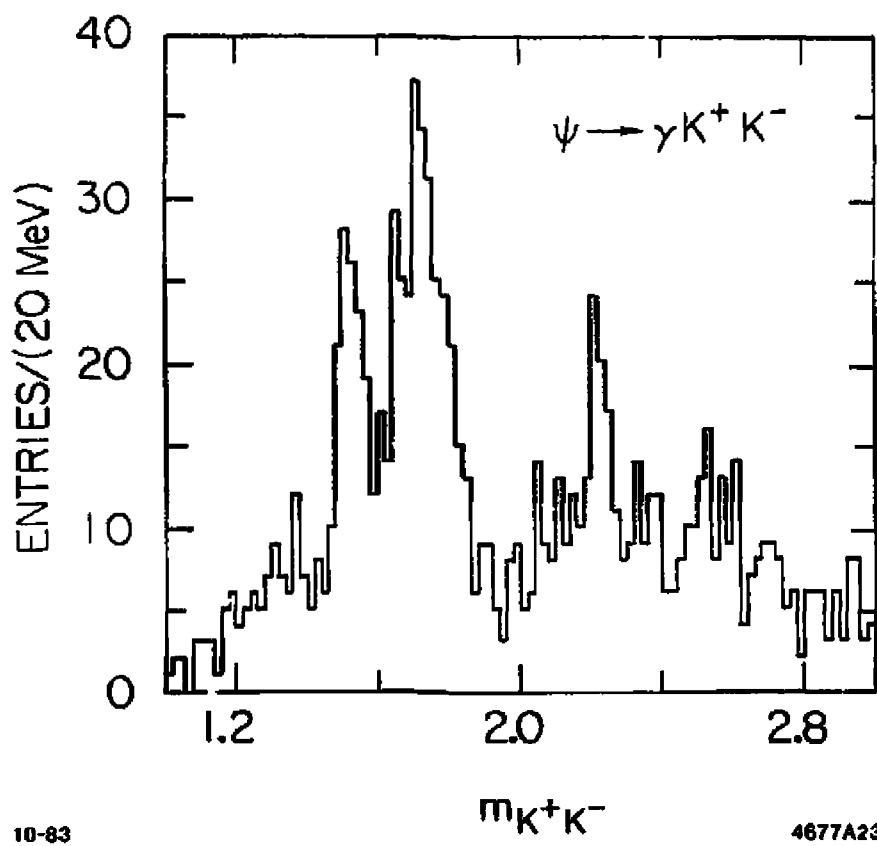


Fig. 22.  $Mass_{K^+K^-}$  (GeV) distribution from  $J/\psi \rightarrow \gamma K^+ K^-$ .

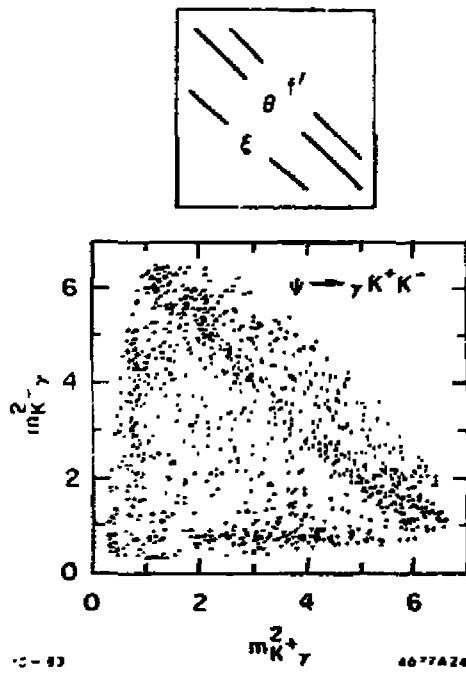


Fig. 23. Dalitz plot  $mass_{K^+\gamma}^2$  versus  $mass_{K^-\gamma}^2$  from  $J/\psi \rightarrow \gamma K^+ K^-$ . The schematic drawing displays the bands of the  $f'(1515)$ ,  $\theta$  and  $\xi$  decays.

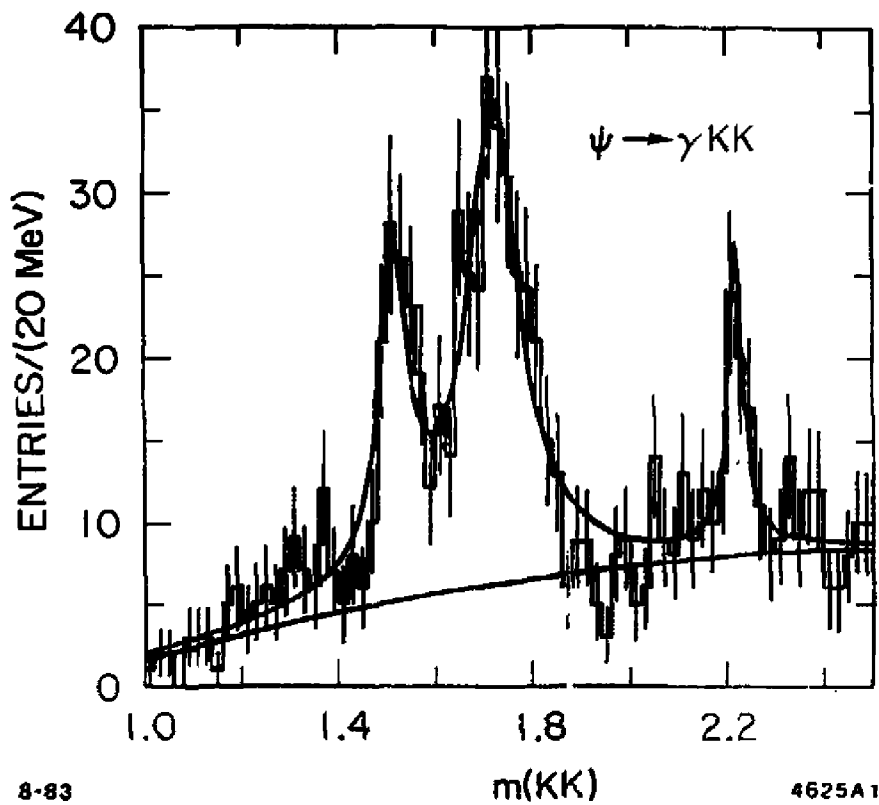


Fig. 24.  $Mass_{K^+K^-}$  (GeV) distribution from  $J/\psi \rightarrow \gamma K^+K^-$  drawn with a fit with three Breit-Wigner curves.

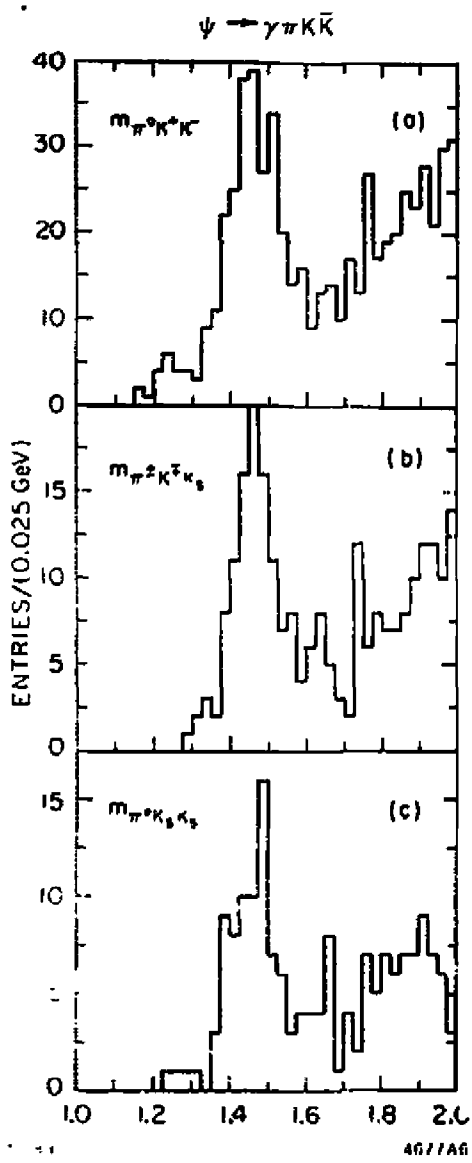


Fig. 25. (a)  $Mass_{\pi^0 K^+ K^-}$  (GeV) distribution from  $J/\psi \rightarrow \gamma\pi^0 K^+ K^-$ .  
 (b)  $Mass_{\pi^\pm K^\mp K_S}$  (GeV) distribution from  $J/\psi \rightarrow \gamma\pi^\pm K^\mp K_S$ . (c)  $Mass_{\pi^0 K_S K_S}$  (GeV) distribution from  $J/\psi \rightarrow \gamma\pi^0 K_S K_S$ .

the  $\pi^0 K^+ K^-$  mode the following values are obtained from a Breit-Wigner fit to the  $\iota$ ,

$$m_\iota = 1.46 \pm .01 \text{ GeV}$$

$$\Gamma_\iota = .097 \pm .025 \text{ GeV}$$

$$\text{BR}(J/\psi \rightarrow \gamma\iota) \times \text{BR}(\iota \rightarrow \pi^0 K^+ K^-) = [5.3 \pm .6(\text{stat}) \pm 1.0(\text{sys})] \times 10^{-3}$$

The fit is shown in Fig. 26. The width is larger than the MARK II and Crystal Ball values because this analysis has no low mass cut on the  $K^+ K^-$  mass. The branching ratios of the other modes are under study. All three branching ratios together will enable a check of the  $\iota$  isospin.

The decay  $J/\psi \rightarrow \gamma\gamma\rho^0$  is studied in the region above the  $\eta'$ . The events are 4-C fit to  $J/\psi \rightarrow \gamma\gamma\pi^+\pi^-$ . Fig. 27 is a scatter plot of mass( $\gamma_{low}\pi^+\pi^-$ ) versus mass( $\pi^+\pi^-$ ). A large  $\rho^0$  signal is observed in a band in the mass( $\pi^+\pi^-$ ). For events with mass,  $1.2 < \text{mass}(\gamma_{low}\pi^+\pi^-) < 1.6 \text{ GeV}$ , the mass( $\pi^+\pi^-$ ) is plotted in Fig. 27(b). The  $\rho^0$  is clearly seen for events above the  $\eta'$ . Requiring the  $\rho^0$  and removing  $\rho\pi$  background, the resulting mass( $\gamma_{low}\pi^+\pi^-$ ) distribution is shown in Fig. 28. The  $\eta'$  is off scale in the vertical scale of the plot. A wide structure above 1.4 GeV is clearly visible. Fitting two Breit-Wigner curves with one fixed at a mass of 1.275 GeV, the following values are obtained, mass =  $1.425 \pm .014 \text{ GeV}$ ,  $\Gamma = .112 \pm .067 \text{ GeV}$ , and  $\text{BR}[J/\psi \rightarrow \gamma X(1.42)] \times \text{BR}[X(1.42) \rightarrow \gamma\rho^0] = [7.4 \pm 2.2(\text{stat}) \pm 1.3(\text{sys})] \times 10^{-5}$ . The Breit-Wigner curve with a fixed mass at 1.275 GeV yields an upper limit for possible decays of  $\eta(1270) \rightarrow \gamma\rho^0$  or  $\eta(1275) \rightarrow \gamma\rho^0$  of  $1.9 \times 10^{-5}$  at 90% C.L. Background investigations and a spin-parity analysis of this structure are currently in progress.

$J/\psi \rightarrow \gamma\eta\pi^+\pi^-$  is studied with 4-C and 5-C fits. After fitting to the 4-C hypothesis  $J/\psi \rightarrow \gamma\gamma\gamma\pi^+\pi^-$ , the scatter plot of mass( $\gamma\gamma\pi^+\pi^-$ ) versus mass( $\gamma\gamma$ ) is plotted in Fig. 29 with 3 entries per event.  $\pi^0$  and  $\eta$  vertical bands are observed. In Figs. 30(a) and (b) the  $\gamma\gamma$  mass is plotted. The  $\pi^0$  and  $\eta$  mass peaks are clearly observed. Cutting on the  $\eta$  peak,  $.475 < \text{mass}(\gamma\gamma) < .625$ , the mass( $\gamma\gamma\pi^+\pi^-$ ) is plotted in Fig. 31(a). Cutting off the  $\eta$  peak,  $.4 < \text{mass}(\gamma\gamma) <$

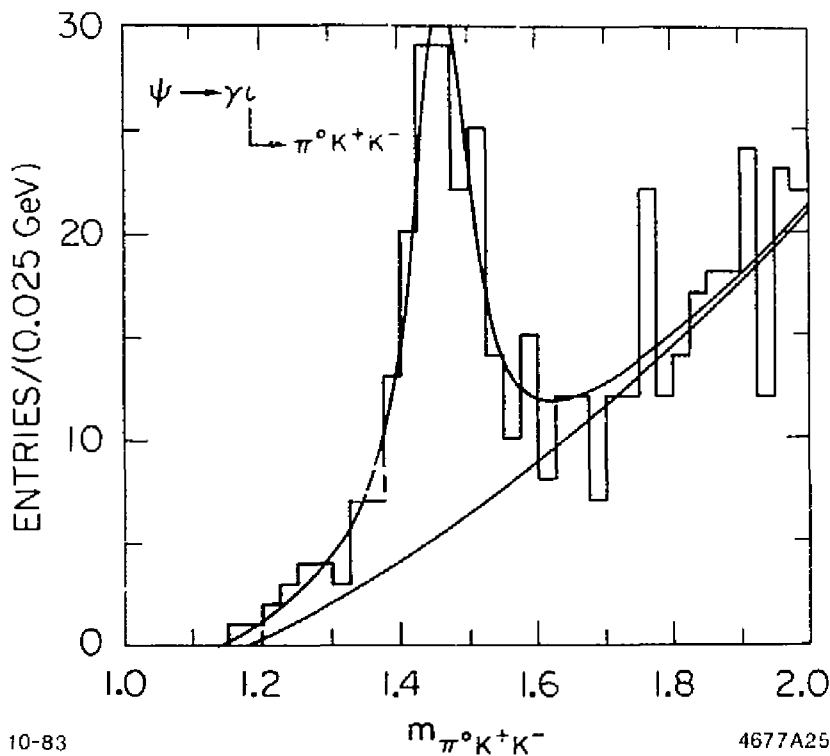


Fig. 26.  $Mass_{\pi^0 K^+ K^-}$  (GeV) distribution fitted to a Breit-Wigner curve from  $J/\psi \rightarrow \gamma \pi^0 K^+ K^-$

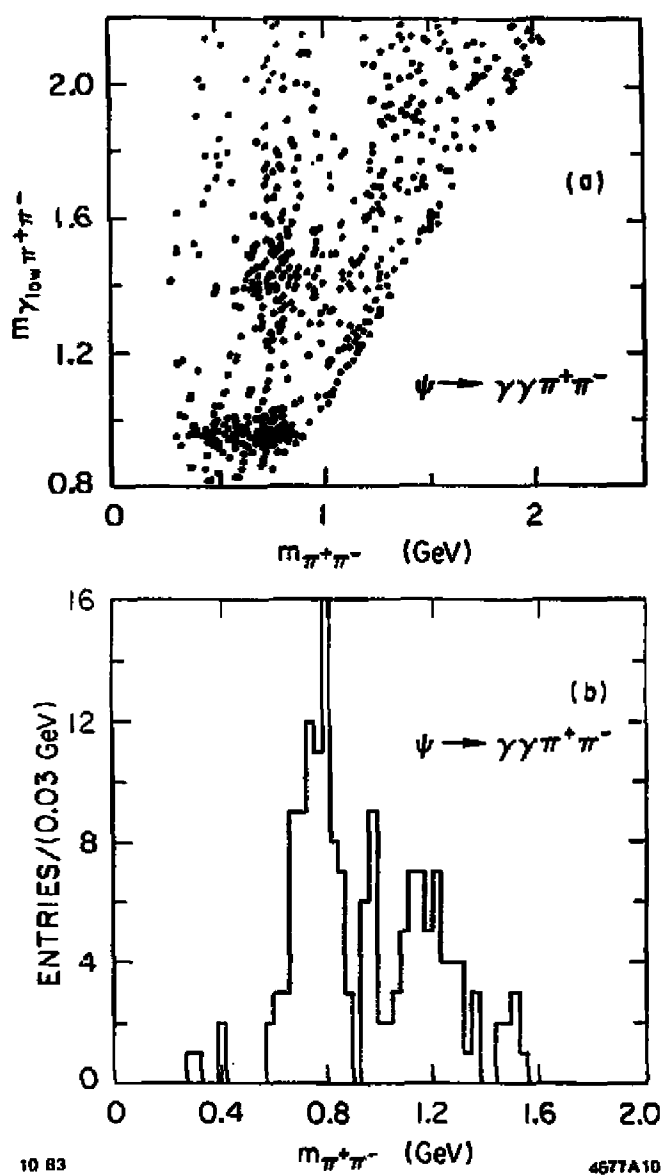


Fig. 27. (a) Scatter plot of  $m_{J/\psi \text{ low}} \pi^+ \pi^-$  versus  $m_{\pi^+ \pi^-}$  from events that fit to  $J/\psi \rightarrow \gamma\gamma\pi^+\pi^-$ . (b)  $m_{\pi^+ \pi^-}$  projection of above plot for events satisfying  $1.2 < m_{J/\psi \text{ low}} \pi^+ \pi^- < 1.6$  GeV.

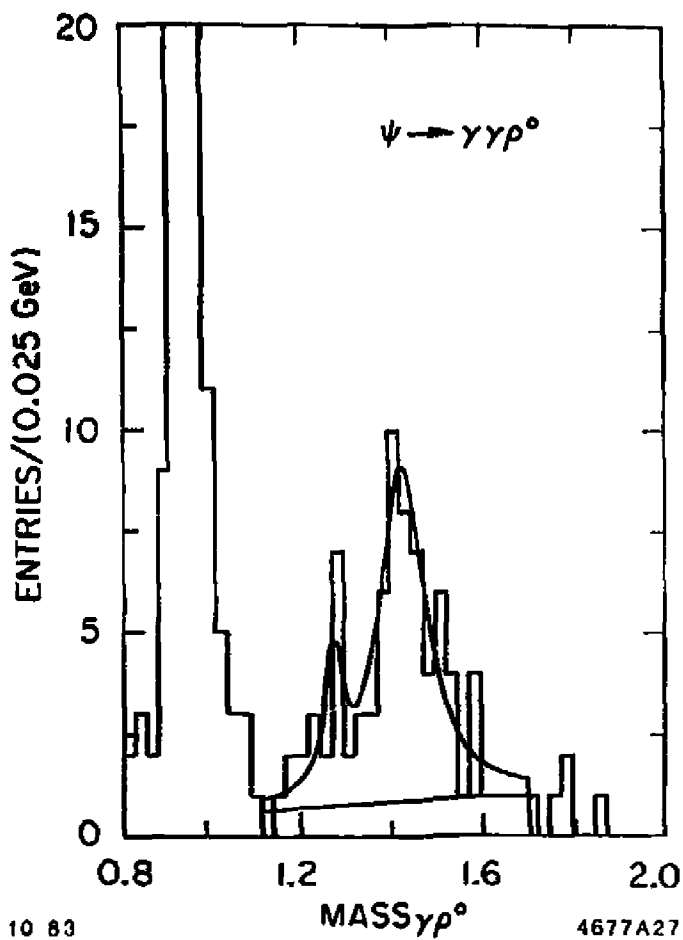


Fig. 28. Mass,  $\rho_0$  (GeV) distribution after requiring that the  $\pi^+ \pi^-$  are from  $\rho^0$  decays. The line is a fit with two Breit-Wigner curves.

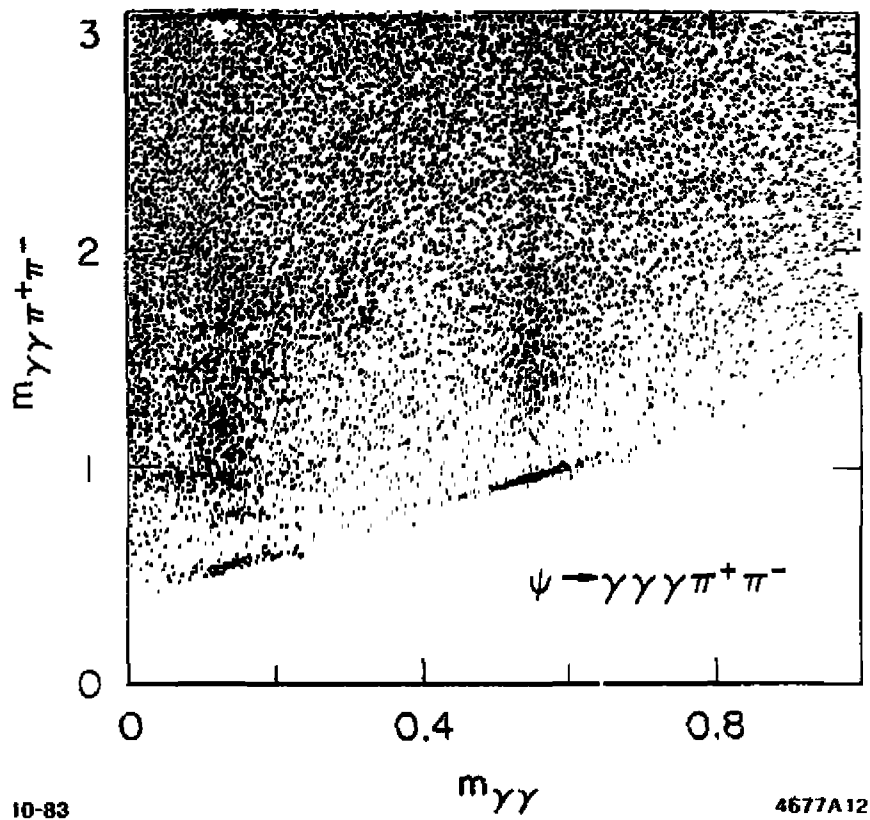


Fig. 29.  $Mass_{\gamma\gamma}$  versus  $Mass_{\gamma\gamma\pi^+\pi^-}$  of events that fit to  $J/\psi \rightarrow \gamma\gamma\pi^+\pi^-$ . There are three entries per event.

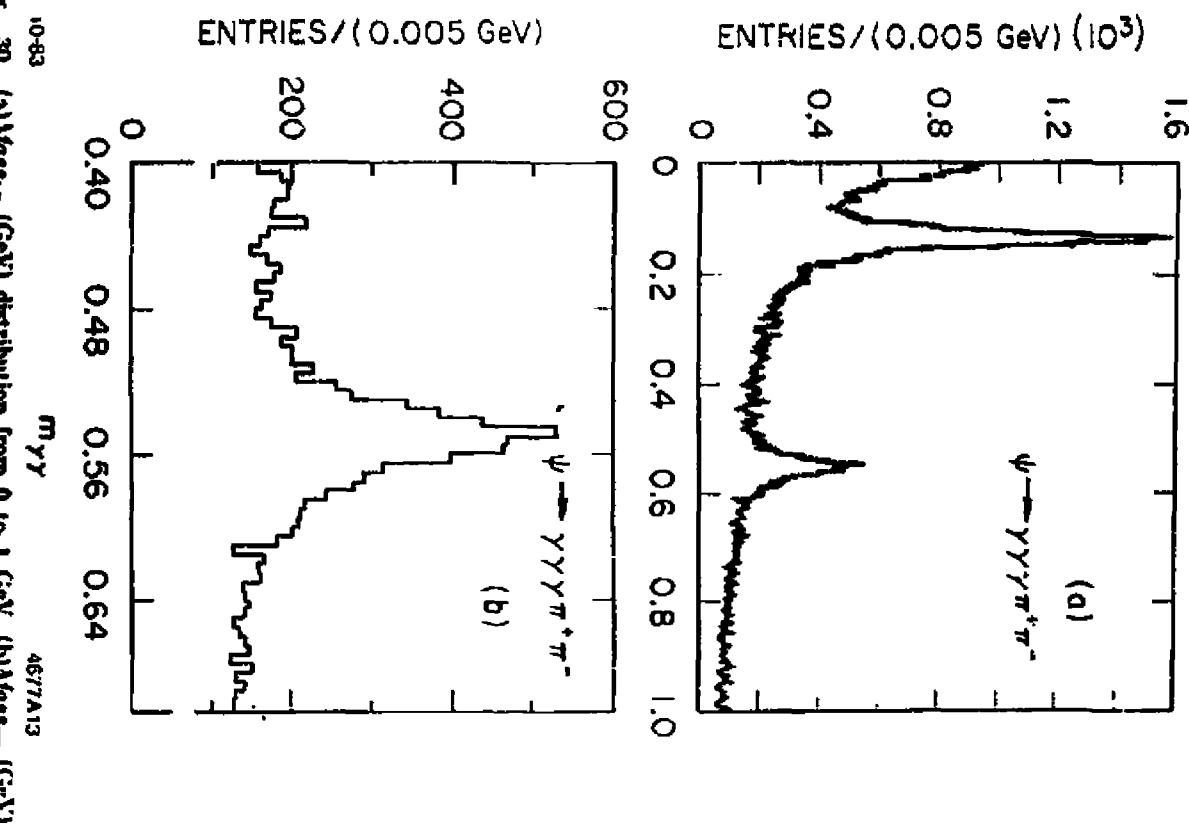


FIG. 30. (a) Mass  $\gamma\gamma$  (GeV) distribution from 0 to 1 GeV. (b) Mass  $\pi^+\pi^-$  (GeV) distribution from 0.4 to 0.7 GeV.

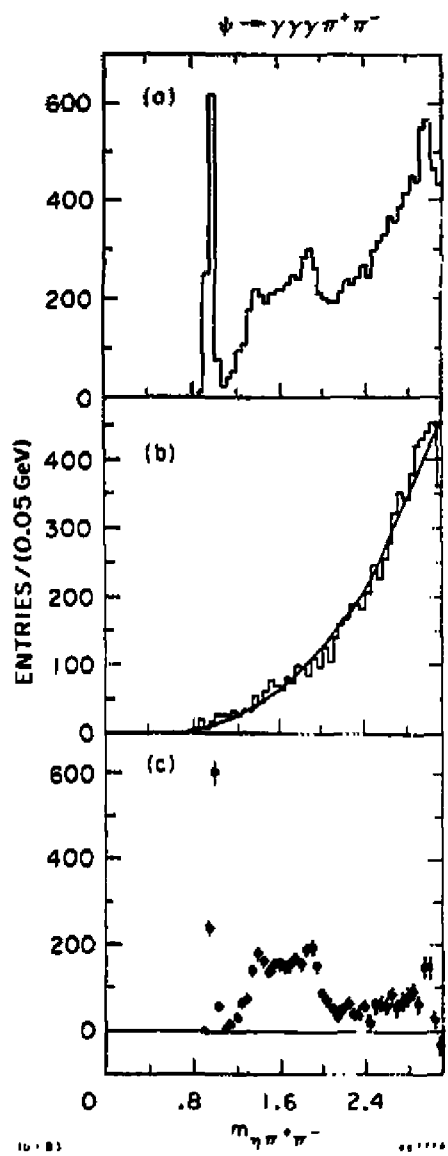


Fig. 31. (a)  $Mass_{\gamma_2 + \pi^-}$  (GeV) distribution when  $.475 < mass(\gamma_1) < .625$ .  
 (b)  $Mass_{\gamma_2 + \pi^-}$  (GeV) distribution when  $.4 < mass(\gamma_1) < .475$  or  $.625 < mass(\gamma_1) < .7$  with a polynomial fit. (c)  $Mass_{\gamma_2 + \pi^-}$  (GeV) distribution, events in plot (a) subtracted by the polynomial fit to events in plot (b).

.475 or .625 < mass( $\gamma\gamma$ ) < .7, the resulting mass( $\gamma\gamma\pi^+\pi^-$ ) is plotted in Fig. 31(b). This represents the combinatorial background signal. It is fitted with a polynomial and most of this background populates the mass region above 2 GeV. To obtain the real  $\eta\pi^+\pi^-$  signal, a polynomial fitted to Fig. 31(b), is subtracted from the events in Fig. 31(a). The resulting plot is shown in Fig. 31(c). The main structures are the  $\eta'$ , a broad structure from 1 to 2 GeV and the  $\eta_c$ . The overall shape appears to be neither a single Breit-Wigner shaped resonance nor phase space. The approximate branching ratio of the entire structure in the 1-2 GeV region is  $7 \times 10^{-3}$ .

Applying a 5-C fit to the events, the Dalitz plot of mass( $\eta\pi^+$ )<sup>2</sup> vs mass( $\eta\pi^-$ )<sup>2</sup> is shown in Fig. 32 for those events with  $1 < \text{mass}(\eta\pi^+\pi^-) < 2$  GeV. The plot shows a clear peak in both modes at  $.08$  GeV<sup>2</sup> which corresponds to decay of the  $\delta$ . Hence the decay  $J/\psi \rightarrow \gamma\delta^\pm\pi^\mp$  is being observed. The mass( $\eta\pi^+\pi^-$ ) is now studied with and without requiring the  $\delta$ . Figs. 33(a), (b) and (c) are mass( $\eta\pi^+\pi^-$ ) distributions from the 5-C fit with no background subtraction. The first one is with no cuts, the second with a "δ cut",  $.93 < \text{mass}(\eta\pi^\pm) < 1.03$ , and the third with an "anti δ cut",  $.93 > \text{mass}(\eta\pi^\pm)$  or  $\text{mass}(\eta\pi^\pm) > 1.03$ . The  $\eta\pi^+\pi^-$  mass plot with the "δ cut", Fig. 33(b), shows no evidence for the  $\iota$  at 1.44 GeV. However there appears to be a structure at 1.38 GeV. The background is not smooth and the shoulder around 1.3 GeV may be the D(1285). A conservative limit that the iota cannot be larger than the number of events at 1.44 GeV in Fig. 33(b) yields the result  $\text{BR}(J/\psi \rightarrow \iota) \times \text{BR}(\iota \rightarrow \delta^\pm\pi^\mp) \times \text{BR}(\delta^\pm \rightarrow \eta\pi^\pm) < 1.1 \times 10^{-3}$  at 95% confidence level. The structure, approximately 50 MeV below where the iota is expected, has been fitted separately to 1 and 2 Breit-Wigner curves with the second resonance in the fit being fixed at the D(1285) mass and width. The fits are applied to the events in Fig. 33(b). The fit to a single Breit-Wigner curve, shown in Fig. 34(a), yields the values, mass =  $1.349 \pm .011$  GeV and  $\Gamma = .147 \pm .036$  GeV. The fit to two Breit-Wigner curves, shown in Fig. 34(b), yields the values, mass =  $1.378 \pm .004$  GeV and  $\Gamma = .027 \pm .018$  GeV. Further reductions of backgrounds in this mode are being studied to improve the iota limit and resolve the emerging structure at 1.38 GeV.

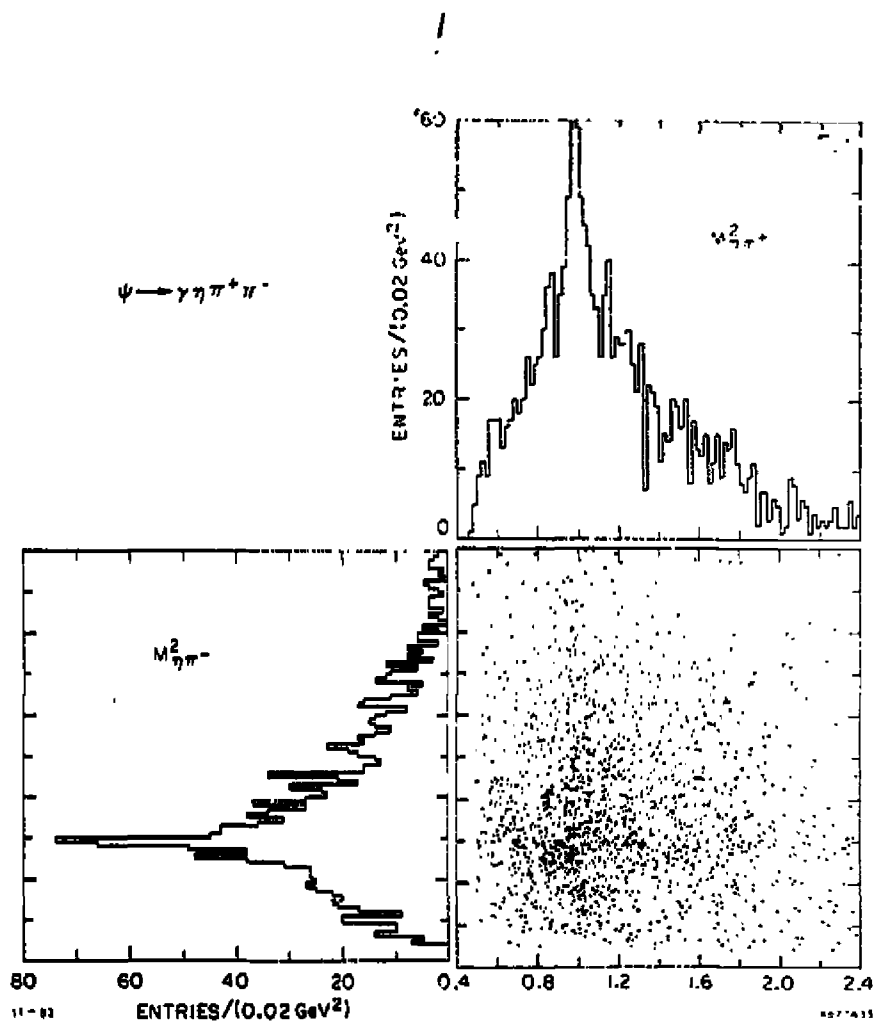


Fig. 32. Dalitz plot of  $M_{\eta_b^+}^2$  versus  $M_{\eta_b^-}^2$  with vertical and horizontal projections.

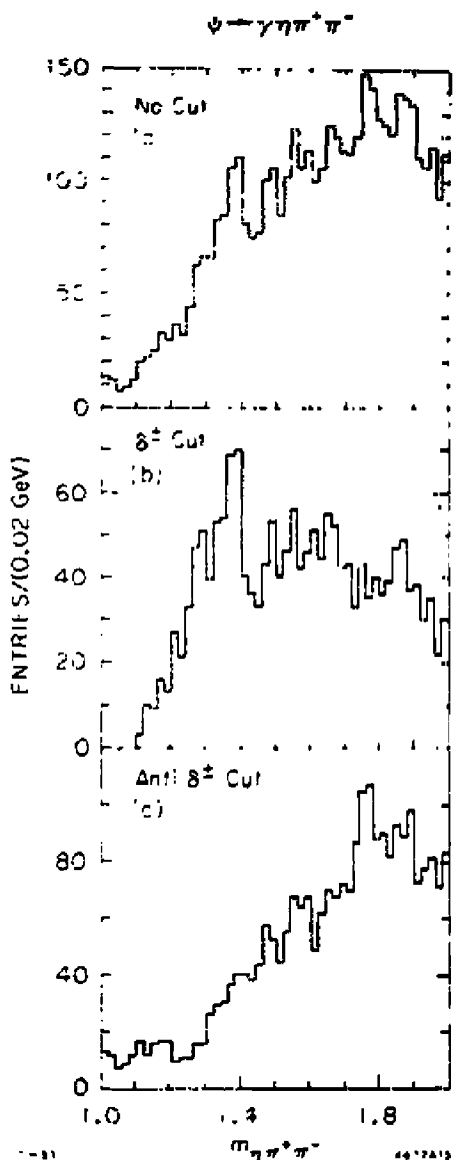


Fig. 33. (a) Mass <sub>$\eta \pi^+ \pi^-$</sub>  (GeV) distribution with no "δ cut" after a 5-C fit. Note that this plot has no background subtraction unlike Fig. 31(c). (b) Mass <sub>$\eta \pi^+ \pi^-$</sub>  (GeV) distribution with the "δ cut" after a 5-C fit. The "δ cut" requires .93 < mass( $\eta \pi^\pm$ ) < 1.03. (c) Mass <sub>$\eta \pi^+ \pi^-$</sub>  (GeV) distribution with the "anti δ cut" after a 5-C fit. The "anti δ cut" requires .93 > mass( $\eta \pi^\pm$ ) or mass( $\eta \pi^\pm$ ) > 1.03.

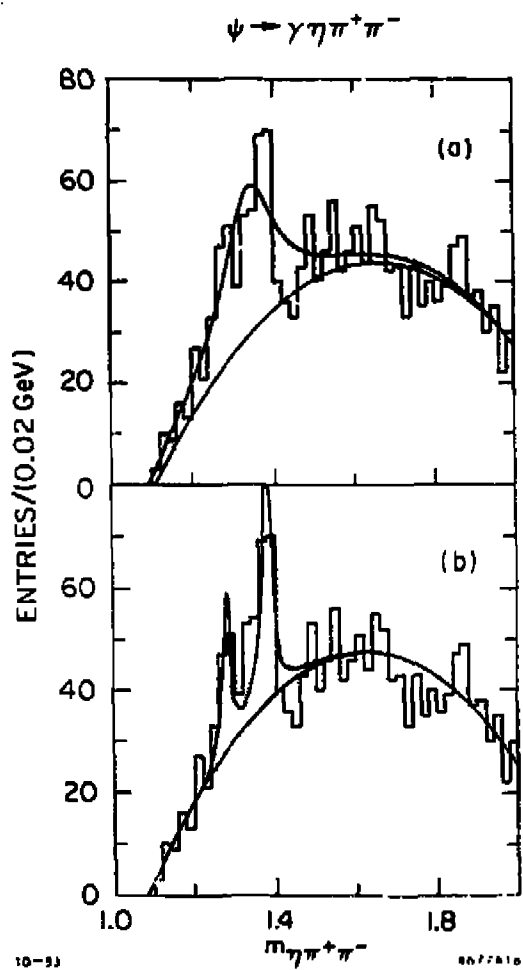


Fig. 34. (a)Figure 33(b) fitted with one Breit-Wigner curve. (b)Figure 33(b) fitted with two Breit-Wigner curves with the second fixed at the D(1285) mass.

## 6. Future Outlook

The preliminary results presented here are from only radiative  $J/\psi$  decays. Studies on  $J/\psi$  hadronic decays are also underway.

MARK III has accumulated  $\sim 6 \text{ pb}^{-1}$  on the  $\psi''$  for producing neutral and charged D's. The present plans are to log another  $9 \text{ pb}^{-1}$  on the  $\psi''$  to bring the total integrated luminosity to  $15 \text{ pb}^{-1}$ . MARK II has accumulated  $2.85 \text{ pb}^{-1}$  in total, hence MARK III should gain a factor of 5 in statistics over previous measurements. The D physics topics MARK III expects to explore are 1) measurements of the ratio of semileptonic branching ratios  $D^0$  to  $D^\pm$ , 2) a possible direct measurement of the ratio of the Kobayashi-Maskawa matrix elements  $V_{cd}/V_{cs}$  from the ratio of  $D \rightarrow \pi e\nu$  to  $D \rightarrow K e\nu$  decays and  $D \rightarrow \rho e\nu$  to  $D \rightarrow K^* e\nu$  decays, 3) new limits on  $D^0 \bar{D}^0$  mixing using  $D^0$  and  $\bar{D}^0$  tagged decays, 4) a study of the mechanism of hadronic weak decays from the relative yields of  $D \rightarrow \pi\pi$ ,  $D \rightarrow K\pi$ , and  $D \rightarrow KK$ , and 5) measurements of the isospin of D decays. MARK III will later have the opportunity of searching for the F, and studying decays of  $\tau$ 's,  $\psi''$ 's, and  $\Lambda_c$ 's.

On the horizon, perhaps by the Summer of 1984, there may be an upgrade of SPEAR with the use of minibeta focusing at the interaction region. Little modification of the MARK III detector will be necessary. It is hoped that the luminosity may be increased by a factor of three. This should have a very important impact on the physics program enabling, for example, the possibility of producing 20 million  $J/\psi$  events at SPEAR in 17 weeks of running. Consequently MARK III looks forward to pursuing and producing interesting and important physics in the next few years at SLAC.

## REFERENCES

1. D. Bernstein *et al.*, Stanford Linear Accelerator Center Report No. SLAC-PUB-3222 (1983).
2. J. Roehrig *et al.*, Stanford Linear Accelerator Center Report No. SLAC-PUB-3199 (1983).
3. J.S. Brown *et al.*, Stanford Linear Accelerator Center Report No. SLAC-PUB-3180 (1983).
4. W. Toki *et al.*, Stanford Linear Accelerator Center Report No. SLAC-PUB-3140 (1983).
5. H. Bledsoe *et al.*, Stanford Linear Accelerator Center Report No. SLAC-PUB-3200 (1983).
6. J.J. Thaler, V.J. Simaitis, J.J. Becker and W.J. Wisniewski, IEEE Trans. on Nucl. Sci. NS - 30, 238 (1978).
7. M. Roos *et al.*, Phys. Lett. 111B, 1 (1982).
8. M. Roos *et al.*, Phys. Lett. 111B, 1 (1982).
9. R. Partridge *et al.*, Phys. Rev. Lett. 45, 1150 (1980).
10. R. Partridge *et al.*, Phys. Rev. Lett. 45, 1150 (1980).
11. T. Himmel *et al.*, Phys. Rev. Lett. 45, 1146 (1980).
12. M. Roos *et al.*, Phys. Lett. 111B, 1 (1982).
13. T.L. Trueman, Phys. Rev. D18, 3423 (1978).
14. N.P. Chang and C.A. Nelson, Phys. Rev. Lett. D40, 1617 (1978).
15. R. Plano *et al.*, Phys. Rev. Lett. D20, 3 (1959).
16. S. Brodsky *et al.*, Phys. Rev. Lett. 73B, 365 (1978).
17. M. Chanowitz, Phys. Rev. D12, 918 (1975).
18. T. Applequist *et al.*, Phys. Rev. Lett. 34, 365 (1975).
19. L. Okun and M. Voloshin, (Moscow, ITEP), ITEP-95-1976 (1976).
20. T. Barnes and F.E. Close, Phys. Lett. 116B, 365 (1982).
21. M. Chanowitz and S. Sharpe, Nucl. Phys. B222, 211 (1983).
22. R. Jaffe and K. Johnson, Phys. Lett. 60B, 201 (1976).
23. D. Scharre *et al.*, Phys. Lett. 97B, 329 (1980).

24. C. Edwards *et al.*, Phys. Rev. Lett. 49, 259 (1982).
25. M. Franklin, Ph.D. thesis, Stanford Linear Accelerator Center Report No. SLAC-254, August 1982.
26. C. Edwards *et al.*, Phys. Rev. Lett. 48, 458 (1982).
27. C. Edwards *et al.*, Phys. Rev. Lett. 51, 859 (1983).
28. D. Burke *et al.*, Phys. Rev. Lett. 49, 632 (1982).
29. M. Roos *et al.*, Phys. Lett. 111B, 1 (1982).